Elevated Anthropogenic Contributions to Trace Elements in Marine Aerosols Compared to Coastal Qingdao in Eastern China

Yuxuan Qi[1,2], Wenshuai Li[1,2,3,4], Wen Qu[5], Haizhou Zhang[5], Wenqing Zhu[6], Jinhui Shi[3,4], Daizhou Zhang[7], Yanjing Zhang[1,2], Lifang Sheng[1,2], Wencai Wang[1,2], Yunhui Zhao[8], Yuanyuan Ma[9], Danyang Ren[10], Guanru Wu[1,2], Xinfeng Wang[11], Xiaohong Yao[3,4], Yang Zhou[1,2*]

[1]State Key Laboratory of Physical Oceanography, Ocean University of China, Qingdao, 266100, China
[2]College of Oceanic and Atmospheric Sciences, Ocean University of China, Qingdao, 266100, China
[3]Key Laboratory of Marine Environment and Ecology, Ministry of Education, Ocean University of China, Qingdao, 266100, China
[4]Laboratory for Marine Ecology and Environmental Science, Qingdao National Laboratory for Marine Science and Technology, Qingdao, 266237, China
[5]North Sea Bureau of Ministry of Natural Resources of the People's Republic of China, Qingdao, 266061, China
[6]Zhongke Tianji Meteorological Technology Co., Ltd., Qingdao, 100193, China
[7]Faculty of Environmental and Symbiotic Sciences, Prefectural University of Kumamoto, 862-8502, Japan
[8]Laixi Meteorological Bureau, Qingdao, 266600, China
[9]Southern Marine Science and Engineering Guangdong Laboratory (Zhuhai), Zhuhai, 519080, China.
[10]Xi'an Meteorological Bureau, Xi'an, 710000, China
[11]Environment Research Institute, Shandong University, Qingdao, 266237, China

Correspondence to: Yang Zhou (yangzhou@ouc.edu.cn)

Abstract. Long-range transport of trace elements (TEs) by aerosols plays a critical role in modulating marine biogeochemistry; however, their source contributions and spatial variability across land-sea gradients remain poorly constrained. Here, we conducted a refined source apportionment of TEs (e.g., Fe, Mn, Cr, V, Ni, Cu, Zn, As, Pb and Cd) in $PM_{2.5}$ collected in the coastal city of Qingdao (eastern China) and adjacent marine regions (the Bohai Sea and Yellow Sea) during spring and summer 2018, to quantitatively resolve terrestrial vs. marine source contributions and identify the key processes controlling their spatial patterns. In spring, all TEs exhibited higher concentrations in Qingdao than in marine atmosphere. In contrast, in summer, Zn, Pb, As, and Cd became more enriched over the marine areas than in Qingdao, with coal combustion accounting for 52.5–78.8% of their concentrations, indicating enhanced anthropogenic impact on the marine atmosphere. For traditional crustal TEs (Fe, Mn and Cr), terrestrial dust dominated in spring Qingdao (e.g., Fe: 81.6%, 2832.0 ng m^{-3}), where the pure dust contributions declined sharply in spring marine areas (Fe: 25.4%, 145.2 ng m^{-3}). However, part of the dust likely underwent aging during transport and was incorporated into the aged marine aerosol factor, which contributed 33.6% of Fe, indicating that dust-related influence remained important offshore and that spring marine aerosols experienced substantial mixing among transported dust, marine processing and anthropogenic emissions. In contrast, coal combustion became the dominant source in summer marine aerosols (Fe: 43.2%, 82.8 ng m^{-3}), exceeding its contribution in Qingdao (Fe: 14.1%, 45.5 ng m^{-3}). Residual oil combustion was identified as the primary source of marine Ni and V (V: 65.7% in spring and 79.8% in summer) and also made substantial contributions to Fe, Mn, and Cr, particularly in summer marine aerosols (e.g., Fe: 26.1%, 50.0 ng m^{-3}). Overall, the refined

source apportionment demonstrates that anthropogenic emissions, especially coal combustion and shipping-related residual oil combustion, play a dominant role in shaping the TE composition of marine aerosols over the Bohai and Yellow Seas, while transported dust and its atmospheric aging remain important for crustal elements.

These results advance our understanding of land-sea interactions in atmospheric TE cycling and provide new constraints for regional air quality and climate models.

1 Introduction

Atmospheric aerosols can significantly impact the local environment and global climate change through modifying the Earth's radiation balance and supplying nutrients to ecosystems (Ramanathan et al., 2007; Choobari et al., 2014; Huang et al., 2014). Anthropogenic activities release pollutants that contribute to atmospheric fine particulate matter ($D_p \leq 2.5$ μm, $PM_{2.5}$). Distinct from large-diameter particles, these primary or secondary $PM_{2.5}$ usually possess long lifetimes, which are capable of undergoing long-range transport and depositing into remote oceans. This process introduces substantial anthropogenic pollutants, thereby impacting ocean ecosystems (Mahowald, 2011; Xu et al., 2021).

Despite trace elements constituting only a minor fraction of the $PM_{2.5}$ mass, their significant post-deposition impacts on downwind marine ecosystems have attracted considerable attention (Li et al., 2015; Morel and Price, 2003; Zhang et al., 2018). Some trace elements deposited in the open oceans, such as Mn, Fe, Ni, Cu, Zn, and Cd, have biological roles, generally as cofactors or part of cofactors of enzymes or as structural elements in proteins (Morel and Price, 2003; Mackey et al., 2012). These elements can markedly influence the growth of phytoplankton taxa and the biological community structure of marine organisms, thereby affecting carbon sequestration and marine primary production (Boyd et al., 2000; Falkowski et al., 1998; Mann et al., 2002; Martin, 1990; Morel and Price, 2003; Yoon et al., 2018; Tang et al., 2021). The total fraction of trace elements cannot be fully utilized by marine biota. In most cases, only the soluble fractions are more likely to be bioavailable (Shi et al., 2012), and the solubility is closely associated with their sources and atmospheric physicochemical processes (Baker et al., 2006; Sholkovitz et al., 2012; Sun et al., 2024; Zhu et al., 2022b). For instance, while mineral dust is the principal source of Fe, numerous studies have demonstrated that Fe emitted from anthropogenic sources has a higher solubility (López-García et al., 2017; Sholkovitz et al., 2012; Sun et al., 2024). Model results also suggest that the combustion-derived Fe tended to account for over 20% of the Fe deposition near the Asian continent, and the efficiency of pyrogenic Fe in enhancing marine productivity exceeds that of lithogenic sources (Ito et al., 2021; Luo et al., 2008). Fe from the combustion source is typically present in finer particles (Buck et al., 2010; Ito and Feng, 2011).

The Bohai Sea (BS) and Yellow Sea (YS) are on the crucial transport pathway for aerosols originating from heavily polluted regions of East Asia to the Northwest Pacific within the westerly belt. Qingdao (QD) is a coastal city adjacent to YS, influenced by both continental and marine air masses (Fig. 1). Aerosol trace elements over the BS and YS likely exhibit distinct characteristics compared to those in coastal cities, necessitating synchronized land-sea observations to investigate these characteristics. However, as previously noted, the current knowledge regarding the source apportionment of trace elements in

marine aerosols remains limited (Hilario et al., 2020). Prior field cruise investigations have focused on the characteristics of total suspended particulates (TSP) and PM_{10} ($D_p \leq 10$ μm) (Hsu et al., 2010b; Li et al., 2025; Peng et al., 2025; Qiu, 2015; Shi et al., 2013; Wang et al., 2013; Yang et al., 2020). In contrast, trace elements in $PM_{2.5}$ have been scarcely explored. It has been revealed that trace elements in fine particles exhibit distinct potential environmental impacts compared with those in coarse particles (Li et al., 2018; Hsieh et al., 2022; Sakata et al., 2022; Zhang et al., 2022), highlighting the importance of targeting $PM_{2.5}$.

Atmospheric processes during long-range transport from the continent to ocean can alter the physicochemical properties of aerosols, thereby influencing the bioavailability of trace elements upon deposition (Schroth et al., 2009; Sholkovitz et al., 2012; Wang et al., 2022; Wang et al., 2021; Luo et al., 2020; Xu et al., 2023; Zhang et al., 2024). Therefore, accurately identifying and apportioning sources of $PM_{2.5}$ and associated trace elements is crucial for understanding their biogeochemical impacts across land-to-sea gradients. This study focuses on the characteristics and source apportionment of elements in $PM_{2.5}$, based on simultaneous observations in Qingdao and over the BS and YS during spring and summer 2018 (Fig. 1). The objective is to provide a more comprehensive understanding of the distribution and sources of trace elements in fine particles from coastal to marginal sea areas in eastern China.

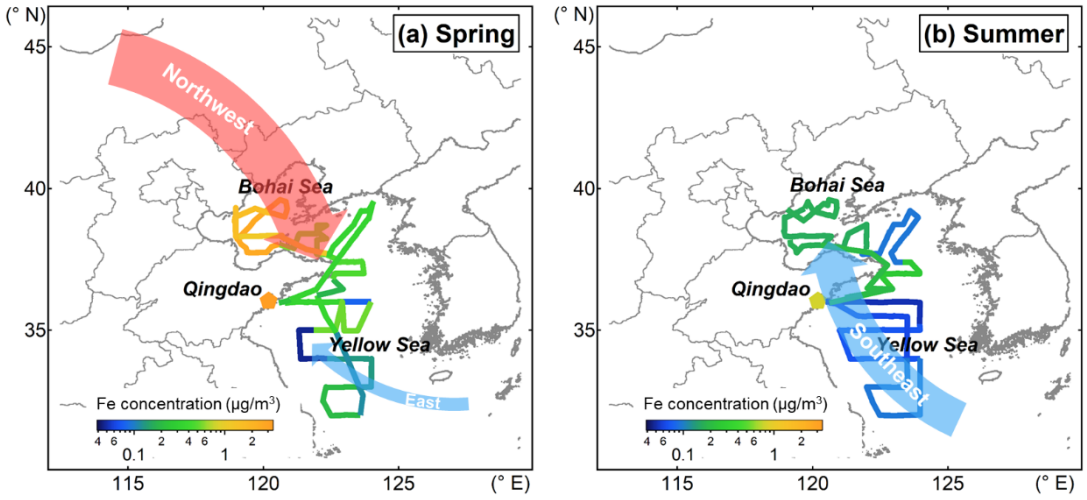

Figure 1: Schematic diagram of regional maps with dominant air mass transport pathways (arrows). The solid lines indicate cruise tracks for (a) springtime and (b) summertime cruises over BS and YS during 2018 and the star denotes the location of Qingdao, with the color-filled indicating Fe concentration.

2 Methodology

2.1 Sample collection

$PM_{2.5}$ samples were collected to measure fine particle components over the BS, YS, and Qingdao during the spring and summer of 2018. In the cruise missions, the samples were collected over the BS and YS from 28 March to 17 April and from 24 July

to 10 August 2018. These areas are located in the downwind areas of the Asian dust source regions and northern China city groups being significantly influenced by dust and anthropogenic pollution (Fig. 1). A total of 18 and 9 samples were collected in spring and summer over the marine areas, respectively. Specifically, these comprised 3 samples from the BS and 15 from the YS in spring, and 2 from the BS and 7 from the YS in summer. Sampling durations varied from several hours to 28 hours in spring and from 18 to approximately 40 hours in summer to accumulate sufficient particle mass. During the collection of marine aerosols, samples were exclusively collected while the ship was underway and the relative wind direction ranged between -60° and +60° (with 0° representing the bow) to avoid contamination from the vessel's own exhaust emissions.

The samples in Qingdao were collected in the same period as the cruise missions. The sampling site was located at the Baguanshan Atmospheric Research Observatory (BARO, 36.03° N, 120.20° E; 74 m above sea level) in the Shinan District Qingdao (Fig. 1), with an approximately 600 m straight-line distance from the coastline (Li et al., 2024; Yang et al., 2024). In Qingdao, 37 and 25 samples were collected during non-rainy periods in spring and summer, respectively. At the coastal site, a day/night sampling strategy was primarily employed, and a few summer samples were collected over about 23-hour periods. High-volume particle samplers (Tisch Environmental, Inc., USA and Qingdao Jinshida Electronic Technology Co., Ltd., China) were applied to collect the particles onto Whatman® 41# filters (Whatman Limited, Maidstone, UK) for trace element analysis, and onto PALL® quartz filters (Pall Gelman, Inc., USA) for analysis of water-soluble ions, organic carbon (OC), and elemental carbon (EC). The 41# filters were washed with diluted acid prior to sampling following Chance et al. (2015) to remove background trace elements. Quartz filters were pre-baked at 450 °C for 6 hours before the sample collection to eliminate background organic contaminants. For quality assurance and control, blank filters were collected and processed, with detailed results and their impact assessment provided in Text S1a and Table S1. All samples were sealed in plastic bags and stored at -20 °C until subsequent analysis.

2.2 Chemical analysis

Trace elements: An 8.0 cm^2 section of both the sample and blank filters was digested with an acid mixture (2.0 mL of 69% HNO_3 and 0.5 mL of 40% HF) in closed Teflon vessels and heated at 180 °C for 48 h. After cooling to room temperature, the solutions were evaporated to near dryness at 180 °C using an electric heating plate (Text S1a). Then, the residue was diluted to 50 mL with 2% HNO_3 and stored at ~4 °C until analysis (Shi et al., 2012; Li et al., 2025).

The concentrations of elements in the extracts were measured using an inductively coupled plasma-mass spectrometry (ICP-MS, iCAP Qc, Thermo Fisher Scientific, Germany) equipped with a quadrupole mass analyzer. Rh, Sc, and Th were used as internal standards to correct for matrix effects and instrumental drift. A standard solution was analyzed as a quality control sample for every 10 samples (Shi et al., 2012).

Water-soluble ions: Sample sections and blank filters were extracted with 10 mL Milli-Q water (≥18.0 MΩ·cm) using ultrasonication for 40 min at 0 °C followed by filtration through a 0.45 μm pore diameter filter, then stored at ~4 °C until analysis in 3 days. Water-soluble ionic species, including Na^+, NH_4^+, K^+, Mg^{2+}, Ca^{2+}, Cl^-, NO_3^-, SO_4^{2-} and $C_2O_4^{2-}$, were analyzed using a Dionex ICS-3000 ion chromatography. To monitor instrumental precision/accuracy and quantify background

contamination over the analytical sequence, blank filter solutions and standard solutions were analyzed every 10 samples (Sun et al., 2024). See Text S1b for additional QA/QC details.

OC and EC: 2.0 cm^2 section of samples and blank filters were analyzed by a Sunset OC/EC analyzer using NIOSH protocol (Wu et al., 2016). The data obtained were calibrated with a standard curve. Detailed information is described in Text S1c.

2.3 Other data and backward trajectories

Meteorological parameters during the sample collection periods, including relative humidity (RH), wind speed (WS) and wind direction, were obtained from the shipboard measurements and Qingdao Meteorological Bureau, and monitoring data of gaseous pollutants, including SO_2, NO_2, O_3, and CO, were from China National Environmental Monitoring Centre (http://www.cnemc.cn/, https://quotsoft.net/air/).

The Hybrid Single-Particle Lagrangian Integrated Trajectory (HYSPLIT) model (PC v4.8) developed by the National Oceanic and Atmospheric Administration Air Resources Laboratory (NOAA-ARL) (Draxler and Rolph, 2014) was employed to reconstruct the three-dimensional 72-h backward trajectories. This was done to identify distinct air mass source regions and their transport paths. The starting point for the trajectory calculations was set at an altitude of 300 m above the ground level. The calculations were performed with the vertical velocity calculation method and archived Global Data Assimilation System (GDAS) meteorological data.

2.4 Positive matrix factorization receptor model

The Positive Matrix Factorization (PMF) model is a widely used receptor model to resolve pollution sources and quantify the source contributions to ambient particulate matter concentrations (Paatero and Tapper, 1994). It decomposes the measured data matrix into factor profile, contribution, and residual matrix. In this study, the Environmental Protection Agency (EPA) PMF version 5.0 was utilized for analysis (Norris et al., 2014).

Source apportionment studies generally follow two complementary approaches: a broad classification of major source categories and a more refined apportionment aimed at resolving mixed sources and atmospheric processes in greater detail. Our study follows the latter approach. Therefore, the PMF analysis was constructed based on the physicochemical interpretability of the bulk $PM_{2.5}$ system, rather than from the perspective of trace metals alone.

Accordingly, the mass concentrations of 12 elements (V, Cr, Mn, Fe, Ni, Co, Cu, Zn, As, Cd, Ba and Pb), 9 water-soluble ions (Na^+, NH_4^+, K^+, Mg^{2+}, Ca^{2+}, Cl^-, NO_3^-, SO_4^{2-} and $C_2O_4^{2-}$), and OC/EC from both Qingdao and cruise campaigns (81 samples) were input to the PMF analysis. Secondary ions and sea-salt related species were retained as process tracers to constrain marine influence, aerosol aging, and internal mixing during transport. Multiple factors ranging from 6 to 10 were thoroughly evaluated to determine the optimal solution. The stability and reliability of the factor solutions were assessed using the displacement (DISP) and bootstrap (BS) uncertainty estimation methods (Norris et al., 2014).

Ultimately, an 8-factor solution emerged as the most robust and interpretable. In contrast, the 7-factor solution failed to distinguish the industrial emissions from dust (Fig. S1a). The 9-factor solution tended to resolve an additional factor; however,

it exhibited relatively low BS mapping values (58%, 67%, and 73%) for several factors (Fig. S1b and Table S2). The 8-factor solution demonstrated the highest stability. The mapping percentages using the BS uncertainty method exceeded 80% for all factors (Table S3), surpassing the performances of the 7-factor and 9-factor solutions (Tables S4 and S2). Moreover, the DISP analysis showed no occurrences of factor swapping and no reduction in the model fit statistic Q (both %dQ and the error code were 0), further validating the stability and interpretation of the 8-factor solution. Detailed information on the PMF performance can be found in Text S2 and Fig. S2. The comparison between measured and PMF-simulated concentrations for representative elements (Fe, V, and Pb) is shown in Fig. S2, with R^2 values of 0.97–0.98 and slopes close to 1.0, demonstrating the strong performance and reliability of the PMF model.

3 Spatiotemporal distributions of trace elements

3.1 Overall concentrations and spatial variations

Figure 2, Tables S5 and S6 summarize the overall average concentrations of elements. Over the BS and YS, the predominant trace elements were Al, Fe, and Zn, with concentrations (average ± standard deviation) of 1043.2 ± 1031.0 ng m^{-3}, 648.6 ± 654.8 ng m^{-3}, and 49.9 ± 75.0 ng m^{-3} in spring, and 71.1 ± 19.0 ng m^{-3}, 109.8 ± 51.4 ng m^{-3}, and 44.9 ± 30.2 ng m^{-3} in summer, followed by Mn (spring) and V (summer) respectively. In the coastal city, the dominant trace elements were Al and Fe, with average concentrations of 5573.5 ± 5641.1 and 3347.3 ± 3249.3 ng m^{-3} in spring and 572.9 ± 395.4 and 228.3 ± 211.7 ng m^{-3} in summer, followed by Mn in spring and Zn in summer, respectively (Fig. 2c). Among the measured anthropogenic trace elements (e.g., Pb, Cu, As, Cd), Zn was the most abundant in both marine and coastal environments, with its anthropogenic origin confirmed by a high enrichment factor (EF; calculation method provided in the Supplement, Text S3 and Fig. S3) (Taylor, 1964). Except for V, element concentrations during summer in Qingdao were lower than those reported by Li et al. (2018) during summer 2016. In this study, V and Ni, as representative tracers of emissions from heavy oil combustion, indicated a higher influence from this source during the campaigns (Li et al., 2020; Zhang et al., 2019b; Zhao et al., 2013).

All elements displayed notably higher concentrations in Qingdao compared to the marine area in spring. However, the discrepancy in concentrations of V, As, and Cd between land and sea was relatively smaller than those of other elements (Fig. 2). The YS region recorded the lowest concentrations for most elements in both spring and summer. Conversely, Zn, As, and Cd exhibited elevated levels over the ocean in summer (Fig. S4b), highlighting the significant impact of transported primary anthropogenic emissions on marine aerosol composition. Notably, a severe pollution event (sample SU005, 1-2 August 2018) under stagnant meteorological conditions (WS < 2 m s^{-1}) led to a pronounced concentration peak of these elements over marine areas. Back trajectory analysis indicates that the air masses originated from the industrial emissions and coal combustion-intensive regions of the BS and Liaodong Peninsula (Fig. S5d), further underscoring the significant impact of transported primary anthropogenic emissions on marine aerosol composition. Given the high sensitivity of the mean to such an extreme outlier, particularly with the limited sample size, this sample was excluded from both the calculation of average values and subsequent PMF analysis.

3.2 Seasonal variations

Seasonally, concentrations of Al, Fe, Mn, and Ba over the BS and YS in spring were 4–35 times and 2–10 times higher than those in summer, respectively. This distinct seasonality can be attributed to dust storms, a frequent phenomenon in northern China during spring (Li et al., 2019). In contrast, Zn, As, and Cd displayed slightly higher concentrations over the BS in summer than in spring, suggesting anthropogenic emissions in the Circum-Bohai-Sea (CBS) region (a geographic area encompassing the land and coastal zones surrounding the BS in China, it includes, but is not limited to, the Bohai Rim) (Polissar et al., 2001). Conversely, V and Pb exhibited no discernible seasonal variations, likely due to the consistent anthropogenic emissions such as industrial and residual oil combustion emissions (Wu et al., 2017). In Qingdao, concentrations of all these elements were notably higher in spring compared to summer (Fig. 2c). Similarly, the EFs of Fe and Mn over the BS and YS in summer were higher than those in Qingdao (Fig. S3), suggesting an enhanced influence of anthropogenic sources in the marine atmosphere during this season. This pattern is further examined in the source apportionment results (Sect. 4.3.1).

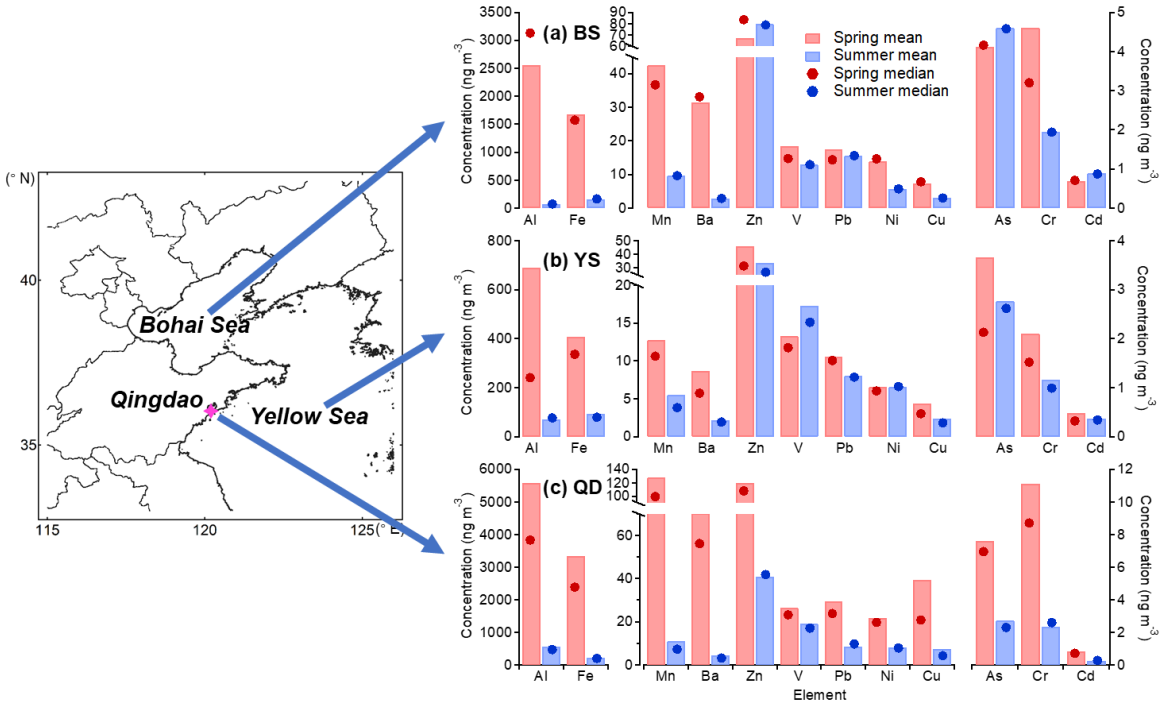

Figure 2: Concentrations of TEs (ng m^{-3}) over the (a) BS, (b) YS, and (c) Qingdao during the campaigns in 2018. The bars represent the time-weighted (hereafter) average, and the circles represent the median.

3.3 Comparison with other studies

We compared our results to other literature data on the concentrations of selected elements in various oceanic regions and typical megacities in China (Tables S5 and S6) (Qi and Zhou, 2021). Notably, elemental concentrations over the YS in this study were significantly lower than those observed during spring 2011 (Zhao et al., 2015). This decrease suggests a potential

reduction in the overall aerosol burden transported to the YS in 2018. It could be a consequence of interannual variations in continental outflow and/or the effectiveness of emission control policies and environmental remediation measures, with the decline in anthropogenic tracers (e.g., Zn, V, Ni, As) providing specific support for the potential role of emission controls. When comparing with spring 2018 ECS sampling data (Sun et al., 2022), a distinct north-to-south decline in the concentrations of mineral elements (Al, Fe, Mn, Ba) and anthropogenic heavy metals (e.g., Zn, Pb) was observed. This spatial pattern suggests that both dust-derived and anthropogenic pollutants, transported via the westerly winds, exert progressively weaker influences on marine aerosols from northern to southern coastal regions (Zhao et al., 2015). Compared with summer island measurements reported by Yuan et al. (2023), the concentrations of most elements in this study were within the same order of magnitude. In Qingdao, most crustal elements, such as Fe and Mn, exhibited higher concentrations in spring and lower concentrations in summer than the annual average concentrations reported in Beijing, Shanghai, and Guangzhou, the typical megacities in China (Table S6) (Chen et al., 2008; Yang et al., 2011). This pattern highlighted the pronounced seasonality of crustal influence in Qingdao, with spring being strongly impacted by dust events, while the input of crustal dust was substantially weakened in summer. Anthropogenic elements such as Zn, Pb, As, Cr, and Cd, which are typically associated with sources like coal combustion, non-ferrous metal smelting, and various industrial processes (Borai et al., 2002; Chen et al., 2013; Karar et al., 2006; Li et al., 2015; Li et al., 2020), were consistently at lower levels in Qingdao than in the three megacities, indicating a lower overall burden from these anthropogenic sources in Qingdao. Notwithstanding the differences in sampling year and season, V concentrations in Qingdao were 2–3 times higher than those in Shanghai (Chen et al., 2008), suggesting a more severe pollution from ship emissions or other residual oil combustions in Qingdao. However, the differences in sampling times need consideration. Sect. 4.2.3 explores the impact of vessel emission control policies on the ship emission aerosols.

4 Discussions

4.1 Source apportionment of $PM_{2.5}$

Eight factors were identified by PMF. The resolved factor profiles and time series are presented in Fig. 3 and Fig. 4 respectively. The time series of individual PMF factor concentrations (e.g., Fig. 4) were derived from the factor contributions output by the PMF model. A factor-specific scaling coefficient was determined by relating the PMF-derived factor contributions to the corresponding absolute concentration. This coefficient was then applied to the full factor contribution time series to reconstruct the absolute concentration time series. The mean concentrations and the relative contributions of each factor are displayed in Fig. 5. The characteristics of the determined aerosol sources are as follows.

Factor 1 was identified as the secondary nitrate factor, characterized by high loadings of NO_3^-, NH_4^+ and Cl^- (Fig.3) (Wu et al., 2017; B. Xu et al., 2023). Based on its chemical profile, this factor represents a mixture of ammonium nitrate and ammonium chloride. This factor contributed a significant proportion of fine particles in both Qingdao and marine environments, accounting for 34.9% and 16.9% of $PM_{2.5}$ mass respectively (Fig. 5b). Notably, Factor 1 displayed an enhanced influence during nighttime (Fig. S6). To help validate the source of this factor, its time-series contribution was compared to ambient gas measurement

data (Fig. 4, and Table S7). It correlated with NO_2 ($r = 0.45$, $p < 0.01$) and CO ($r = 0.39$, $p < 0.01$). This could potentially be indicative of the nocturnal heterogeneous reaction formation or subsequent regional transport (Wang et al., 2018).

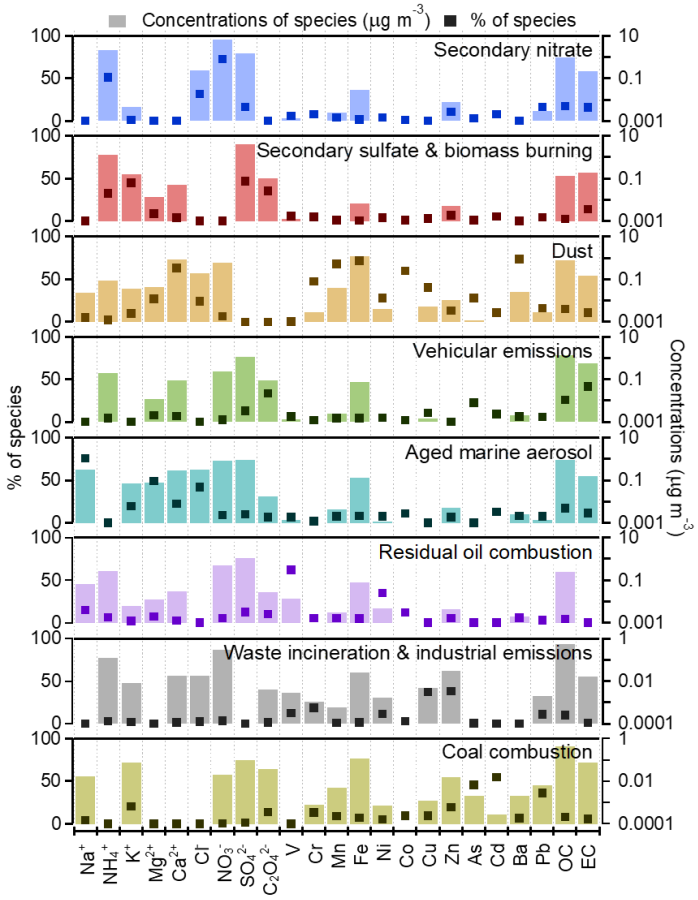

Figure 3: PMF resolved source profiles (dark points represent the percentages and light rectangles represent the concentrations of each species in each factor) of the 8-factor solution.

Factor 2 was recognized as the secondary sulfate & biomass burning (sulfate & BB) factor, marked by high SO_4^{2-}, K^+, NH_4^+ and oxalate (Wu et al., 2017; B. Xu et al., 2023). This factor accounted for 19.4% and 24.3% of the $PM_{2.5}$ mass in Qingdao and marine regions respectively. The notable presence of K^+, oxalate, and some EC and Zn in this factor suggested the possible mixing with emissions from biomass burning (Wang et al., 2018; Zhu et al., 2022). Factor 2 exhibited correlations with CO ($r = 0.54$, $p < 0.01$) and RH ($r = 0.36$, $p < 0.01$). CO serves as a key tracer of primary incomplete combustion processes (Zhang et al., 2017). The strong interconnection between sulfate and oxalate can be ascribed to their similar liquid phase formation mechanisms (Yu et al., 2005; Zhou et al., 2015).

Factor 3, identified as the dust factor, was characterized by high loadings of crustal species, including Ba, Fe, Mn and Ca^{2+} (Fig. 3) (Amil et al., 2016; Gugamsetty et al., 2012; Mustaffa et al., 2014). A significant portion of Co was also apportioned

to Factor 3, denoting its crustal origin (Wu et al., 2023). In Qingdao, the time series of Factor 3 exhibited distinct peaks on 29–30 March, 3, 6, 10–11, and 15 April 2018 (Fig. 4a), each coinciding with documented springtime Asian dust events (Li et al., 2023; Li et al., 2019). Diurnally, Factor 3 exhibited a moderate positive correlation with WS ($r = 0.43$, $p < 0.05$) in Qingdao in spring. Throughout the entire sampling campaign, it maintained a strong negative correlation with RH ($r = –0.72$, $p < 0.01$; Table S7) in Qingdao. These correlations suggested the influence of meteorological conditions, consistent with the inherently arid nature of dusty air masses. Factor 3 accounted for 13.6% of the total $PM_{2.5}$ mass at coastal site and diminished to 1.7% within the marine environments (Fig. 5b).

Factor 4 was identified as the vehicular emissions factor, characterized by significant apportionments for EC and OC, contributing 10.4% to the total Qingdao aerosol mass and 17.6% to the marine aerosols. OC and EC are major pollutants stemming from gasoline and diesel combustion (Liu et al., 2016; Liu et al., 2020). The presence of Cu was likely due to additives in fuel/lubricant combustion, brake linings and tire wear (Gu et al., 2011; Lee et al., 2006; Pant and Harrison, 2013), further supporting this identification. During summertime, vehicular emissions correlated strongly and positively with NO_2 ($r = 0.78$, $p < 0.01$). Throughout the sampling campaign, the factor correlated positively with CO ($r = 0.30$, $p < 0.05$) and negatively with O_3 ($r = –0.37$, $p < 0.01$). These relationships underscored the chemical interplay where O_3 is reduced by NO to generate NO_2.

Factor 5 was characterized by high concentrations of marine source components, including Na^+, Mg^{2+} and Cl^-, and showed a positive correlation with WS ($r = 0.35$, $p < 0.01$) and a strong negative correlation with RH ($r = –0.63$, $p < 0.01$) (Sharma et al., 2016; Zhang et al., 2018). These features aligned with sea salt aerosols production driven by wind-induced disturbance of the ocean surface (Prijith et al., 2014). However, the coexistence of nitrate, sulfate, and harbour-related components (Ca^{2+}, K^+) suggested that this factor did not represent fresh sea spray, but rather aged marine aerosol mixed with anthropogenic pollutants during transport (van Pinxteren et al., 2010; Pey et al., 2013; Liu et al., 2025). At the coastal site, its enhanced daytime concentration was consistent with the sea-land breeze patterns (Fig. S6). Time series analysis further showed that Factor 5 had a prevalent influence over the BS and YS (Fig. 4). Notably, in Qingdao during spring, the synchronous peaks of Factor 5 and Factor 3 strongly suggest mixing between marine aerosol and dust during transport. This interpretation is consistent with the prevailing westerly and northwesterly winds (Fig. 1 and Fig. S5a), which favor the co-transport of continental dust and marine aerosols to the coastal sampling site. A representative example is shown by backward trajectories for a marine sample (SP012, with the highest aged marine aerosol source concentration) and its corresponding Qingdao samples during the same period. These trajectories clearly illustrate that the air masses originated from the YS and approached Qingdao from the west prior to their arrival at the sampling site (Fig. S7). Moreover, high wind speeds during dust events may also enhance sea salt emissions (Feng et al., 2017), further contributing to the similarity in the temporal variations of dust and aged marine aerosol. On average, the aged marine aerosol factor contributed 9.9% to $PM_{2.5}$ mass at the Qingdao site and 22.1% in marine $PM_{2.5}$ samples.

Factor 6, the residual oil combustion factor, was characterized by high apportionments of V and Ni (Wu et al., 2020), contributing 6.6% and 9.0% to the total $PM_{2.5}$ mass in Qingdao and BS and YS areas, respectively. The cargo handling capacity of Qingdao port reached 542.5 million tons in 2018, ranking fourth among the main ports of China (data obtained from China

Statistical Yearbook, 2018, https://data.stats.gov.cn/easyquery.htm?cn=C01). The contributions of Factor 6 highlighted the significant influence of shipping traffic on both the coastal city Qingdao and the BS and YS areas. It showed a positive correlation with SO_2 ($r = 0.38$, $p < 0.01$) (Table S7), further validating its association with ship emissions (Zhang et al., 2019b). Factor 7 was defined as the waste incineration & industrial emissions factor. It exhibited substantial loadings of heavy metals such as Zn, Cu, Cr, and Pb, which are tracers of waste incineration & industrial activities, including metallurgical smelting, oil mining, and the production of cement, plastic, pigment, chemical and building materials (Borai et al., 2002; Karar et al., 2006; Li et al., 2012; Tian et al., 2012; Wang et al., 2018). Its correlations with NO_2 ($r = 0.50$, $p < 0.01$) and SO_2 ($r = 0.31$, $p < 0.05$) underscored its industrial origins, although it is a minor contributor to total $PM_{2.5}$ (3.1% in Qingdao and 1.5% in the BS and YS areas, as shown in Table S7).

Factor 8 was identified as the coal combustion factor. This attribution was robustly supported by the enrichment of well-documented coal combustion tracers of As, Cd and Pb, elements consistently linked to coal-fired emissions (Chang et al., 2018; Li et al., 2020; Rai et al., 2016; Zhang et al., 2011; Zhang et al., 2008). Furthermore, the factor exhibited a statistically significant correlation with SO_2 ($r = 0.35$, $p < 0.01$), a primary gaseous co-emission from coal combustion (Lin et al., 2022). This coal combustion factor contributed modestly to the total $PM_{2.5}$ mass but showed notable spatial variability: 2.1% at coastal (Qingdao) site and 4.8% in marine $PM_{2.5}$ samples, with marine contributions exceeding twice the coastal value. The spatial distributions of coal-fired power plants, $PM_{2.5}$ emissions from coal-fired power plants, and atmospheric As concentration in China collectively indicated that the coal combustion factor was mainly associated with transport from coastal source regions (Fig. S8) (Tian et al., 2014; Wang et al., 2016; Zhang et al., 2020). In particular, the dense concentration of coal-fired power plants along the coastline serves as a persistent source of coal-burning aerosols over the sea. Under prevailing winds, emissions from these coastal plants can be transported offshore, resulting in elevated concentrations over marine areas. However, these coal-related sources were not consistently located upwind of the Qingdao sampling site and therefore have minimal influence on concentrations there. Furthermore, although this factor contributed only a limited fraction of $PM_{2.5}$ mass, it made a substantial contribution to heavy metal concentrations, which will be discussed in detail in Sect. 4.3.

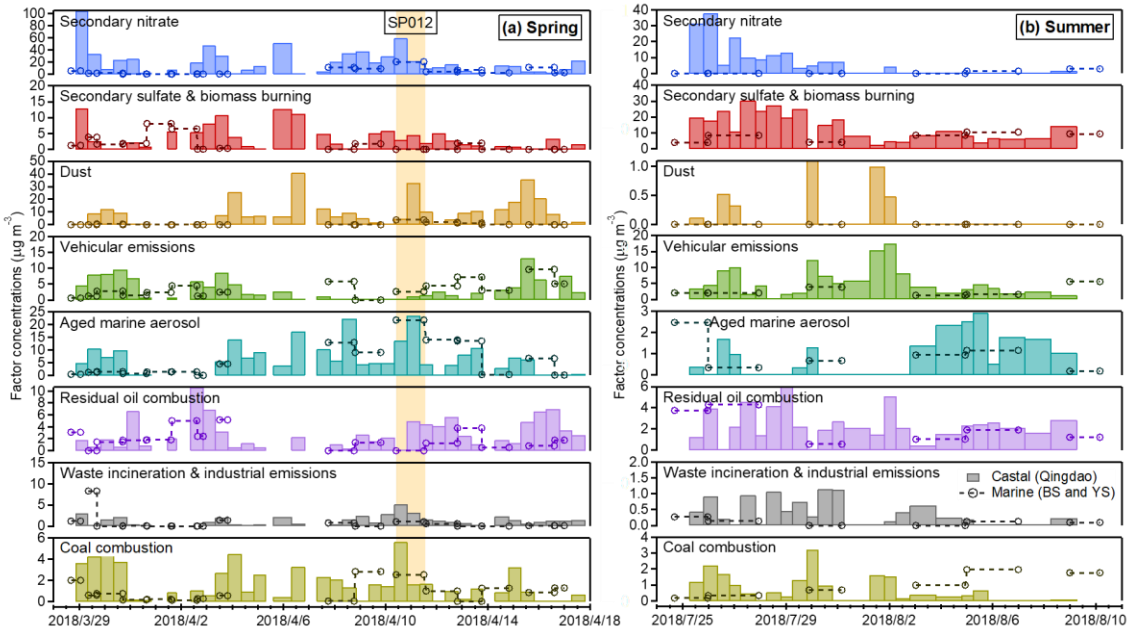

Figure 4: Time series of individual PMF factor concentrations for $PM_{2.5}$ in (a) spring and (b) summer. Bars represent coastal (Qingdao) samples, while open circles with dashed lines denote marine (BS and YS) samples. "SP012" marked in (a) shows the factor concentrations during the sampling period of sample SP012. The detailed procedure for converting the model's factor contribution output to concentrations is provided in Sect. 4.1.

4.2 Difference and linkage in source contributions of $PM_{2.5}$ between coastal and marine environments

4.2.1 Enhanced anthropogenic inputs to marine areas driven by spring westerly

Distinct differences in $PM_{2.5}$ source apportionment were observed between the coastal and marine environments during spring. Secondary nitrate, dust, and waste incineration & industrial emissions exhibited significantly lower concentrations and relative contributions in marine environments compared to the coastal site. Specifically, secondary nitrate was the predominant contributor at the coastal site, accounting for 41.6% (20.4 μg m^{-3}) of $PM_{2.5}$ mass. In contrast, its contribution was notably lower in the marine area (23.6%, 4.4 μg m^{-3}; Fig. 5). This disparity was driven by the divergence in the air masses transport pathways. Air masses arriving at Qingdao (spring clusters E, S, W and summer cluster L) contained higher concentrations of secondary components like NO_3^- and NH_4^+ (land-based species), which did not fully extend to marine areas (Fig. S5a and c, and Table S8). As NO_3^- and NH_4^+ are primarily associated with terrestrial sources, their influence is more significant in Qingdao.

Dust, the second largest contributor in spring, accounted for 19.6% (9.7 μg m^{-3}) in Qingdao but sharply reduced to 2.7% (0.5 μg m^{-3}) over the BS and YS. Dust particles with larger diameters are more likely to be removed through inertial and gravitational settling processes during transport (Gu et al., 2011; Vu et al., 2015; Zhao et al., 2015), leading to the rapid sedimentation and reduced concentration in remote marine environments (Baker and Jickells, 2006; Ma et al., 2023). The waste incineration & industrial emissions factor also showed lower contributions in the marine area (2.0%) compared to the coastal site (3.5%).

Aged marine aerosol, sulfate & BB, coal combustion, vehicular emissions and residual oil combustion showed higher contributions in the marine area, despite lower or comparable absolute concentrations to the coastal site (Fig. 5). Aged marine aerosol contributions were 30.9% in the marine area, versus 13.0% at the coastal site, consistent with the fact of its marine origin. Furthermore, its temporal peaks at Qingdao closely resembled those of the dust factor (Fig. 4a). It is hypothesized that during dust events, aged marine aerosol may mix with the transported dust, making the two factors difficult to distinguish and leading to the higher concentration of aged marine aerosol at Qingdao (6.4 μg m^{-3}) compared to those over the marine area (5.7 μg m^{-3}).

On the one hand, increased RH in marine air favored the formation of sulfate and oxalate through liquid-phase reactions (Zhang et al., 2019a; Zhou et al., 2015), enhancing sulfate & BB contribution in the marine atmosphere (9.9%) compared to the coastal site (7.1%). On the other hand, small-sized particles from biomass burning and coal combustion are more effectively transported to marine areas (Gu et al., 2011; Vu et al., 2015). The vehicular emissions, accounting for 17.9% in marine areas (Fig. 5b), had nearly identical average concentrations in both Qingdao and marine environments (3.4 and 3.3 μg m^{-3}, respectively) (Fig. 5a). Characterized by small EC-rich particles, these vehicular emissions can be easily transported to remote areas (Gu et al., 2011; Vu et al., 2015). As shown in Figs.4a, S8a and c, time series peaks of vehicular emissions factor over the ocean coincided with the samples collected from air masses originating in northern and central China, i.e., samples SP010, SP014, and SP017.

Residual oil combustion exhibited a lower average concentration in marine areas (1.7 μg m^{-3}) than in Qingdao (2.9 μg m^{-3}). This is consistent with the influence of ship and port emissions on coastal urban areas. The time series peaks of residual combustion factor over the ocean were often associated with air masses transported from sea to land (e.g., samples SP006 and SP008). Unlike the waste incineration & industrial emissions factor, these four anthropogenic factors demonstrated that varying transport paths, particle size, and source proximity could affect land-sea distribution patterns of their contributions.

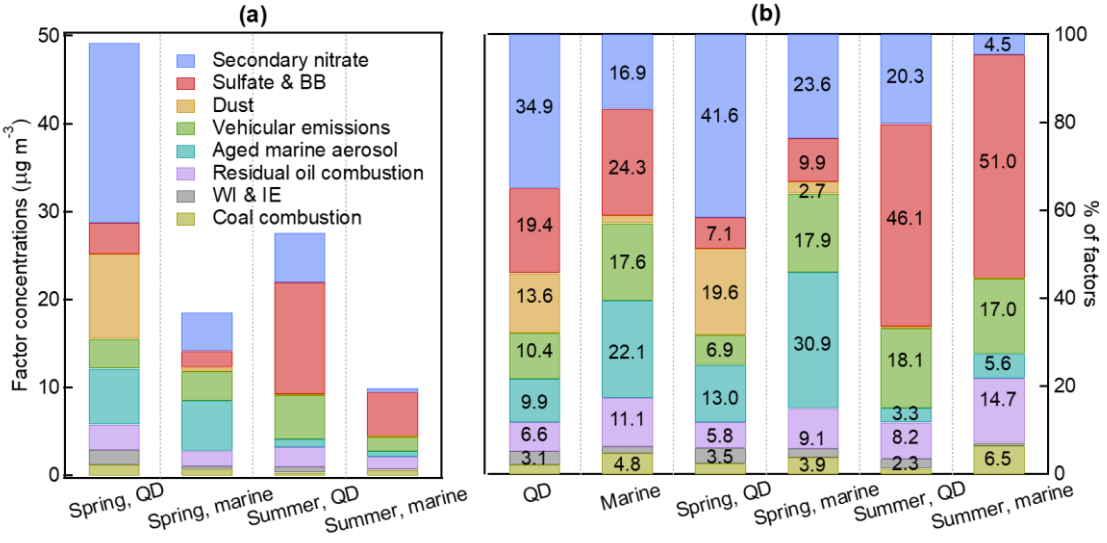

Figure 5: The averaged (a) concentrations and (b) relative percentage contributions of identified source factors to $PM_{2.5}$ as determined by PMF analysis. Sulfate & BB refers to sulfate & biomass burning. WI & IE denotes waste incineration & industrial emissions. "marine" refers to the BS and YS.

4.2.2 Dominance of biomass burning and vehicular emissions in summer marine areas

Similar spatial land-sea distribution patterns were observed for secondary nitrate, dust, waste incineration & industrial emissions, as well as sulfate & BB in summer. However, the dominant contributor shifted from secondary nitrate in spring to sulfate & BB in summer, indicating decreased nitrate contributions during the warmer season. This reduction was attributed to the thermal decomposition of NH_4NO_3 under high summer temperatures and enhanced secondary sulfate facilitated by photochemical reactions with the high temperature and sufficient light, as well as aqueous-phase oxidation promoted by high RH (Wu et al., 2017; Kim et al., 2022).

Unlike in spring, summer data revealed higher concentrations and contributions of vehicular emissions at the coastal site (5.0 μg m^{-3}, 18.1%) compared to the BS and YS (1.7 μg m^{-3}, 17.0%) (Fig. 5). This difference could be ascribed to the seasonal variations in pollutants transport direction, driven by the summer southeasterly winds, altering typical land to sea trajectories. Similarly, aged marine aerosol concentrations were higher at the coastal site (0.9 μg m^{-3}) compared to marine areas (0.6 μg m^{-3}), which may be partly attributed to enhanced sea spray generation near the shoreline due to stronger wave breaking (Zhou et al., 2025); summer southeasterly winds may also facilitate marine aerosol transfer inland, thereby influencing the air quality of coastal urban areas (Figs.S4c, d, and S8d). The coal combustion factor also showed a more pronounced contribution over the marine area (0.6 μg m^{-3}, 6.5%) than at the coastal site (0.4 μg m^{-3}, 1.3%). This variation was attributed to elevated concentrations of trace elements in marine aerosols during summer.

4.2.3 Changes over the past decade

Comparative analysis of particulate matter source apportionment between the present study and earlier work (Wu et al., 2017) suggested evolving trends in source contributions over the past decade. Notably, statistical comparison is not feasible due to the lack of primary data from the earlier study. The observed differences showed an increase in the fraction of secondary nitrate (from 25.2% to 34.9%), a decrease in sulfate (& BB) (from 25.7% to 19.4%), and minimal change in vehicular emissions contribution (from 10.0% to 10.4%), accompanied by an elevation in the mass concentrations of Ni and V. These observed variations were consistent with the impacts of evolving environmental regulations and the transformation in the energy structure over the past decade.

Another interesting trend is the contribution from residual oil combustion. As a coastal city, Qingdao experiences heavy shipping traffic. Results from a PMF analysis conducted from August 2018 to May 2019 near the Qingdao Port indicated that marine vessel emissions were the primary contributor (25.1%), with the YS and BS as potential source regions (Bie et al., 2021). In this study, residual oil combustion accounted for 6.6% at the coastal site and 11.1% over the marine area. The cargo handling capacity of Qingdao ports in 2017 was approximately double that of 2007 (China Statistical Yearbook, 2018 and 2008, https://data.stats.gov.cn/easyquery.htm?cn=C01), underscoring the significant impact of ship emissions.

The implementation of "domestic emission control areas" (DECAs) in China signified a significant regulatory shift to address air quality concerns. Commencing on January 1, 2017, ships berthed at core ports in three designated regions (the Pearl River Delta, the Yangtze River Delta, and the Bohai Rim) were mandated to use fuel with a sulfur content not exceeding 0.5% (DECA 1.0) (Zhang et al., 2019b). This regulation was further expanded on January 1, 2019 to require vessels operating within 12 nautical miles of the coastline to adhere to the same low sulfur criteria (DECA 2.0) (Yu et al., 2021). The transition to low-sulfur fuels led to a significant increase in the Ni/V ratio of emitted aerosols. This phenomenon was primarily caused by the desulfurization of fuels which removed V much more efficiently than Ni, thereby increasing the Ni/V ratio in the fuel itself, which is then reflected in the combustion emissions (Yu et al., 2021). In Shanghai, the Ni/V ratio in ship emitted particles derived from PMF increased from 0.34 to 0.45 between DECA 1.0 and DECA 2.0, reaching 2.14 in 2020 (Yu et al., 2021). In the present study, the Ni/V ratio for residual oil combustion aerosols resolved by PMF was 0.37, aligning with DECA 1.0 levels. Notably, Bie et al. (2021) reported a Ni/V ratio of 2.17 in 2019 near the Qingdao Port, confirming DECA policy effectiveness. The lower Ni/V ratio (0.37) in our study suggested residual oil combustion pollutants in the study area may still include higher-sulfur fuel signatures, potentially from regional transport rather than strictly regulated local shipping.

4.2.4 Comparison with source apportionment studies in other marginal seas of the Western Pacific

We compared the source apportionment results obtained over the BS and YS in this study with those from studies conducted over the offshore eastern China Sea, around the Taiwan Island, China, and over the South China Sea (SCS) (Sun et al., 2022; Yen et al., 2022a; Yen et al., 2022b). These sea areas all belong to the marginal seas of the Western Pacific, sharing the common influence of the East Asian monsoon and continental outflows, yet exhibiting differences in the types of pollution sources and their respective contributions. Although direct comparison should be interpreted with caution because of differences in sampling period, receptor location, and PMF inputs among studies, the available results still reveal meaningful regional similarities and contrasts.

Across these marginal seas, $PM_{2.5}$ sources were generally resolved into secondary inorganic aerosols, dust-related sources (including crustal or fugitive dust as reported in other studies), marine source (including sea salt or oceanic spray), and specific anthropogenic emissions. Among these, secondary aerosols (dominated by nitrate and/or sulfate) and marine-related source were important contributors in most regions. For example, secondary formation (22.9%) and combustion source (30.6%) were reported to make significant contributions over the offshore eastern China Sea in spring (Sun et al., 2022; Fig. S9c), which is qualitatively similar to our findings for spring and summer. Likewise, the notable contribution of marine-related aerosol in this study (22.1%) is comparable to that reported for other sea areas, including 18.6–30.2% around Taiwan Island and 5.6–29.5% over the SCS annually (oceanic spray over the Dongsha Islands; oceanic spray & fugitive dust over the Nansha Islands) (Yen et al., 2022a; Yen et al., 2022b; Fig. S9a, b, and d).

In contrast, the BS and YS showed a stronger continental influence, as reflected by the clearer resolution of industrial processes and coal combustion related factors. This characteristic was less pronounced over the more southerly sea areas, suggesting a stronger impact of the industrial structure and coal-dominated consumption of Northern China on the marine regions.

Furthermore, vehicular emissions were identified as an important and stable pollution source over the BS and YS (17.6%) in spring and summer, aligning with the substantial contribution (24.5%) reported over the offshore eastern China Sea in spring (Sun et al., 2022). In contrast, studies around the Taiwan Island and over the SCS more commonly resolved a mixed factor combining ship and vehicular emissions, with contributions of 17.4–41.2% annually (Yen et al., 2022a; Yen et al., 2022b). This difference may indicate that traffic and shipping emissions were more readily separated over the BS and YS, although part of the discrepancy may also arise from differences in receptor environments and PMF configurations among studies. Overall, the comparison suggests a clear transition in $PM_{2.5}$ source characteristics from the BS to the YS, with continental anthropogenic influences gradually weakening and marine-related contributions becoming more important southward/offshore, while the adjacent seas of the Western Pacific further reflect increasing impacts from mixed marine and shipping-related emissions.

4.3 Source contributions of individual elements

This study revealed clear disparities in the source contributions to the ten essential elements across terrestrial and marine regions, mirroring the spatial distribution patterns seen in $PM_{2.5}$ (Fig. 6, Fig. S10, Table S9 and S10). The influence of dust and waste incineration & industrial emissions sources decreased, whereas coal combustion, vehicular emissions (in spring) and aged marine aerosol exhibited enhanced contributions to elements over the marine area.

4.3.1 Fe, Mn and Cr

Atmospheric aerosols containing Fe and Mn are crucial for marine biogeochemistry and ecosystem dynamics. As a limiting nutrient, Fe is closely coupled with sulfur cycles (e.g., via dimethyl sulfide production/processing) in both the atmosphere and ocean, triggering phytoplankton blooms, and enhancing carbon dioxide (CO_2) sequestration through the global carbon cycle (Shi et al., 2012; Zhuang et al., 1992). Similarly, Mn serves as an essential cofactor for enzymes involved in photosynthesis and other biochemical processes, making it vital for marine organisms, and its deficiency directly impacts the growth rate of phytoplankton (Morel and Price, 2003; Hawco et al., 2022).

In spring, dust was the dominant source of Fe and Mn in Qingdao, contributing 81.6% and 78.6% to the total Fe and Mn, respectively (Fig. 6a and b). Over the marine region, however, the contribution of dust decreased substantially, to 25.4% for Fe and 23.4% for Mn. This significant reduction in the relative contribution of dust over the ocean suggests substantial processing and mixing during transport. Indeed, the PMF model identified “aged marine aerosol” as a distinct source, which contributed 33.6% to Fe and 29.7% to Mn in marine aerosols during spring (Fig. 6a and b). This factor is characterized by strong correlations between sea salt ions and crustal elements (e.g., Fe, Mn), coherent temporal variations, and consistent backward trajectory clusters, indicating substantial mixing of mineral dust with sea spray aerosols (SSAs) during transport (Geng et al., 2014; Hilario et al., 2020). This behavior aligns with previous single-particle observations, showing that mineral dust can be efficiently incorporated into SSA particles during long range transport over the ocean (Andreae et al., 1986; Okada et al., 1990; Zhang et al., 2003; Zhang et al., 2006; Wagener et al., 2008; Hsu et al., 2010a; Adachi et al., 2020; Knopf et al.,

2022; Kwak et al., 2022). The implications of such internal mixing for Fe bioavailability remain uncertain. While SSAs could inhibit Fe dissolution via pH buffering (Hsu et al., 2010a), organic ligands in SSAs may also promote the release and stabilization of soluble Fe (Wu et al., 2023). Since dissolved Fe was not measured in this study, we do not attempt to quantify this effect, but note that SSAs mixing is a non-negligible process in the marine Fe budget.

In contrast to dust, the relative contributions from vehicular emissions (11.0% and 10.6% for Fe and Mn, respectively) and coal combustion (16.2% and 19.5%), were markedly higher in marine aerosols than in Qingdao (vehicular emissions: 1.8% and 1.8%; coal combustion: 4.9% and 6.2%). In terms of absolute concentrations, coal combustion contributed 92.4 ng m^{-3} Fe and 4.0 ng m^{-3} Mn to the marine atmosphere in spring, while dust contributed 145.2 ng m^{-3} Fe and 4.8 ng m^{-3} Mn (Fig. S10 and Table S10).

In summer, coal combustion became the primary contributor to marine Fe and Mn (43.2% and 46.5%, respectively), exceeding Qingdao contributions by 3 times. This finding is consistent with higher EFs of Fe and Mn observed over the BS and YS in summer compared to Qingdao (Fig. S3), further supporting the enhanced influence of anthropogenic sources in the marine atmosphere during this season. Residual oil combustion was also a discernible source for Fe and Mn in summer marine atmosphere, contributing 26.1% (50.0 ng m^{-3}) and 24.4% (1.9 ng m^{-3}), respectively. Southeasterly winds transported ship-derived pollutants coastward, markedly increasing the relative contributions of Fe (24.1%) and Mn (22.9%) in Qingdao compared to spring (2.8% and 3.1%, respectively). However, from the perspective of absolute concentration, the contributions of residual oil combustion to Fe and Mn in Qingdao remained lower in summer (77.8 and 2.9 ng m^{-3}, respectively) than in spring (98.7 and 3.7 ng m^{-3}). A t-test on the concentrations showed that these seasonal differences are not statistically significant ($p > 0.05$), suggesting that emissions from residual oil combustion remain relatively stable, likely associated with persistent shipping activities and stationary sources.

Comparisons with previous studies regarding Fe and Mn show both consistencies and discrepancies. Chen et al. (2024) also identified dust as the dominant source of Fe in Qingdao during spring, with a contribution of 88%, which is comparable to our estimate of 81.6%. In contrast, Zhang et al. (2024) reported substantially higher dust contributions over the YS in spring (52–69%) than observed in this study (25.4%) over the BS and YS, together with higher contributions from industry and coal combustion (25.4–33.6% vs. 17.6%), whereas the contribution from ship emissions was broadly comparable (0.9–8.2% vs. 10.2%). Compared with Zhang et al. (2024), our results suggest a more differentiated source structure, particularly over the BS and YS, where continental outflow appears to be shaped by mixing among industrial emissions, coal combustion, vehicular emissions, secondary processing, and marine aerosol during transport. Notably, Zhang et al. (2024) did not explicitly resolve the mixing of marine aerosol with transported dust or separate several additional anthropogenic sources. If the aged marine aerosol factor identified here is considered as part of the aged dust-influenced aerosol during transport, the total dust-related contribution would increase to 59.0%, making our results broadly comparable to those of Zhang et al. (2024). Zhang et al. (2024) provided a first-order classification of major source categories, whereas our refined PMF analysis resolves additional source and process complexity and thus offers a more detailed representation of transported aerosols over the marginal seas. The seasonal pattern of Mn source apportionment reported by Yang et al. (2022) for Beijing is also consistent with our results

for Qingdao, with dust dominating in spring and industrial emissions becoming more important in summer. Notably, our source apportionment revealed a significant contribution of anthropogenic source to total Fe and Mn in the marine atmosphere, accounting for 41.0% in spring and 90.3% in summer for Fe, and 46.9% and 7.8% for Mn (Fig. 6a, b, and Table S9).

The source pattern of Cr shared some similarities with that of Fe and Mn in spring (Fig. 6c). Marine aerosols exhibited a pronounced increase in coal combustion contributions (30.0% in spring and 49.1% in summer) compared to Qingdao particles, likely due to emissions from coastal power plants transported seaward. Waste incineration & industrial emissions was the second-largest contributor to Cr in Qingdao during spring and the largest contributor during summer, qualitatively similar to the findings of Yang et al. (2022) for Beijing, although the industrial emissions contribution levels they reported (41%–77%) were substantially higher than those in our study (15.3% in spring, 27.3% in summer). Direct comparisons for Cr over the marginal seas are limited, which highlights the need for further research on the speciation and sources of this trace metal in marine environments.

4.3.2 Ni, Cu, Zn, V and Cd

Ni, Cu, Zn, and Cd can influence phytoplankton growth dynamics, modify marine biotic community structure, and affect carbon sequestration processes, functioning either as enzyme cofactors or structural elements in proteins (Jickells et al., 2005; Morel and Price, 2003; Shelley et al., 2015). Notably, Ni and V primarily originated from residual oil combustion, with contributions being markedly higher over the marine area (46.2–79.8%) compared to the coastal site (26.2–64.8%) (Fig. 6d and e). However, the absolute concentrations of Ni and V from residual oil combustion were higher in the Qingdao atmosphere (Ni: 4.8–6.0 ng m^{-3}, V: 12.8–16.2 ng m^{-3}) than in the BS and YS atmosphere (Ni: 3.1–3.6 ng m^{-3}, V: 8.2–9.6 ng m^{-3}). This demonstrated that the emissions from residual oil combustion had a significant impact not only on the marine environment but, more notably, on the coastal urban air quality.

Over the BS and YS, coal combustion (21.3–41.2%), vehicular emissions (26.5–29.2%) and WI & IE (13.9–35.3%) contributed more significantly to Cu (Fig. 6f). In Qingdao, WI & IE was an important source of Cu, consistent with observations in Beijing (Yang et al., 2022). Apart from the aged marine aerosol contributions, Zn was associated with multiple anthropogenic sources, including waste incineration, industrial emissions, coal combustion, biomass burning, and secondary sulfate-related aerosol processing. Similar findings have been widely reported in previous PMF studies, where Zn was identified in biomass burning and secondary aerosol factors (Li et al., 2007; Li et al., 2020; Liu et al., 2020; Zhu et al., 2022a; Liu et al., 2025). In the marine area, coal combustion dominated Zn contributions, accounting for 31.5% and 52.5% of total Zn in spring and summer, respectively (Fig. 6g).

4.3.3 Pb, Cd and As

Pb, Cd, and As, which are biologically toxic, pose potential non-carcinogenic or carcinogenic risks to human health and cause considerable detriment upon marine ecosystems (Nagajyoti et al., 2010; Zhang et al., 2018). Source apportionment revealed that coal combustion was the dominant contributor of Pb and Cd in BS and YS areas, particularly during summer, accounting

for 71.6% of Pb and 78.8% of Cd (Fig. 6h and i). The absolute concentrations revealed the land-to-sea transport: coal combustion contributed 4.6 ng m^{-3} of Pb to the marine atmosphere in summer, which was 1.8 times higher than its concentration in Qingdao (2.6 ng m^{-3}), clearly indicating the pervasive influence of terrestrial coal emissions across the sea. In Beijing, the predominant sources of Pb were coal combustion in spring and industrial emissions in summer (Yang et al., 2022), mirroring our coastal observations. Similarly, coal combustion was identified as the primary source of As (34.6–75.0%), with its influence increasing over the BS and YS during spring (59.7%) and summer (75.0%) (Fig. 6j). The emission inventory also indicates that 74.2% of As emissions can be ascribed to coal combustion in China (Tian et al., 2015). Furthermore, vehicular emissions also contributed significantly to As (12.3–56.6%), which can be attributed to the role of As as a recognized tracer for fossil fuel combustion (Chen et al., 2013). An interesting finding was the significant contribution of aged marine aerosol to Zn, Pb and Cd in marine environments during spring, indicating the mixing between SSAs and anthropogenic aerosols. The time series suggested that the peaks in aged marine aerosol contributions coincided with the high concentrations of Pb, Cd and Zn (Figs.4a and S3a), supporting that aged marine aerosol particles acted as a carrier for these toxic anthropogenic elements during transport.

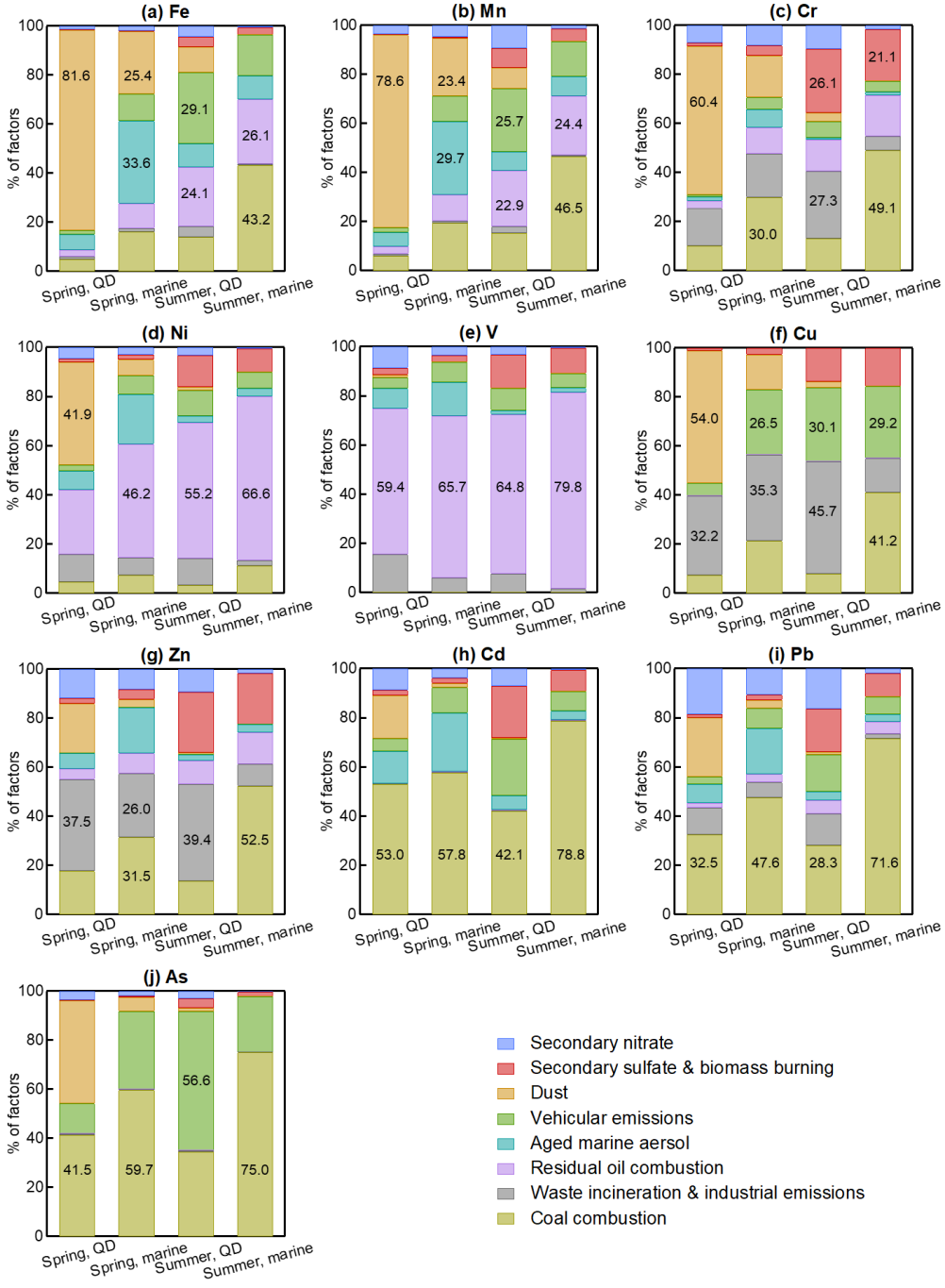

530 **Figure 6: Percentage contributions of various source factors to individual elements based on PMF results. "marine" refers to the BS and YS.**

5 Conclusions

This study investigated the spatial and seasonal distributions, and sources of TEs in $PM_{2.5}$ based on simultaneous observations in Qingdao and over the BS and YS during spring and summer 2018, with a focus on land-sea contrasts and the influence of anthropogenic activities on the marine air. A refined PMF analysis identified eight aerosol sources, including secondary nitrate, secondary sulfate & biomass burning, dust, vehicular emissions, aged marine aerosol, residual oil combustion (ship emissions), coal combustion, and waste incineration & industrial pollutants.

Terrestrial-marine aerosol source gradients were driven by atmospheric transport and deposition processes. Secondary nitrate, primarily derived from terrestrial anthropogenic activities, exhibited a sharp land-to-sea decline, with contributions decreasing from 41.6% (Qingdao) to 23.6% (marine) in spring, and from 20.3% to 4.5% in summer. In contrast, secondary sulfate & biomass burning contributions increased slightly from Qingdao to marine areas: from 7.1% to 9.9% in spring, and from 46.1% to 51.0% in summer, reflecting enhanced sulfur precursor availability in marine areas and long-range transport over the marine areas. Natural terrestrial sources (dust and dust-anthropogenic mixtures) demonstrated pronounced attenuation over marine areas due to size-dependent particle settling. For example, dust contributions declined from 19.6% (Qingdao) to 2.7% (marine) in spring. In contrast, finer anthropogenic particulates (e.g., vehicular emissions) exhibited enhanced offshore transport, with marine contributions (17.9%) exceeding those in Qingdao (6.9%) in spring. Summer southerly winds moderated this land-to-sea contrast. Marine-related aerosols, particularly aged marine aerosols and residual oil combustion, dominated marine areas, with residual oil combustion contributing up to 9.1% in spring and 14.7% in summer.

Trace element distributions mirrored aerosol source dynamics but with source-specific seasonal shifts. All TEs exhibited notably higher concentrations in Qingdao compared to marine in spring, where Zn, Pb, As, and Cd reversed this land-to-sea pattern in summer (marine > Qingdao), reflecting intensified anthropogenic influence over the marine atmosphere. In terms of sources distribution, traditional crustal TEs (Fe, Mn, Cr) were mainly controlled by terrestrial dust in spring in Qingdao (Fe: 81.6%, 2832.0 ng m^{-3} ; Mn: 78.6%, 92.7 ng m^{-3}; Cr: 60.4%, 6.9 ng m^{-3}), but dust contributions decreased sharply over marine areas (Fe: 25.4%, 145.2 ng m^{-3} ; Mn: 23.4%, 4.8 ng m^{-3}; Cr: 16.9%, 0.4 ng m^{-3}). Instead, coal combustion became the dominant source of these elements, particularly in summer marine areas (Fe: 43.2%, 82.8 ng m^{-3}; Mn: 46.5%, 3.6 ng m^{-3}; Cr: 49.1%, 0.6 ng m^{-3}). Residual oil combustion was also the dominant source of Ni and V in both coastal and marine environments (except spring Qingdao Ni, 41.9% sourced from dust), and contributed substantially to Fe, Mn and Cr, particularly in summer (Fe: 24.1%, 77.8 ng m^{-3} in Qingdao and 26.1%, 50.0 ng m^{-3} marine; Mn: 22.9%, 2.9 ng m^{-3} in Qingdao and 24.4%, 1.9 ng m^{-3} marine).

Springtime marine environments also showed elevated aged marine aerosol contributions to Fe, Mn, Zn, Cd, and Pb (18.5–33.6%), indicating extensive multi-source mixing (dust-marine-anthropogenic) in aerosols. The biogeochemical impact of this complex mixing on the reactivity of elements warrants further investigation.

These findings underscore the complex interplay of natural and anthropogenic drivers shaping coastal aerosol composition, and highlight the critical role of atmospheric transport and source-receptor dynamics as key controls on land-to-sea aerosol-

borne element distributions and continental-marine aerosols interactions. This study improves our understanding of how continental emissions influence offshore air quality and marine atmospheric chemistry, which is critical for refining regional air quality and climate models. Future work should further investigate the physicochemical reactivity and solubility of these TEs mixed-source aerosols to assess their impactions for marine biogeochemistry.

Data availability. The backward trajectories were calculated using the Hybrid Single-Particle Lagrangian Integrated Trajectory (HYSPLIT) transport model (https://www.ready.noaa.gov/HYSPLIT.php). The data associated with the figures in this manuscript, including Supporting Materials, are available in the in-text data citation reference Zhou (2026).

Author contribution.

YQ: formal analysis, writing-original draft, validation, writing-review & editing. **WL:** investigating, formal analysis, validation. **WQ:** methodology. **HZ:** methodology. **WZ:** investigating, formal analysis, validation. **JS:** writing-review & editing, methodology. **DZ:** validation, writing-review & editing. **YZ:** investigation, validation. **LS:** validation, writing-review. **WW:** validation, writing-review. **YZ:** investigation, validation. **YM:** investigation, validation. **DR:** investigation, validation. **GW:** investigation, validation. **XW:** methodology. **XY:** validation, methodology. **YZ:** conceptualization, writing-review & editing, validation, funding acquisition, supervision, project administration.

Competing interests. The authors declare that they have no conflict of interest.

Acknowledgments.

This research was sponsored by the National Natural Science Foundation of China (NSFC) (No. 42475119 and 41605114) and Shandong Provincial Natural Science Foundation (No. ZR2024MD016). The authors would like to thank all the colleagues who participated in these campaigns for their support. Data acquisition and sample collections were supported by NSFC Open Research Cruise (Cruise No. NORC2018-001), funded by Shiptime Sharing Project of NSFC. This cruise was conducted onboard R/V *DONGFANGHONG 2* by Ocean University of China. The authors gratefully acknowledge the NOAA-ARL for providing the HYSPLIT transport and dispersion model.

References

Adachi, K., Oshima, N., Gong, Z., de Sá, S., Bateman, A. P., Martin, S. T., de Brito, J. F., Artaxo, P., Cirino, G. G., Sedlacek III, A. J., and Buseck, P. R.: Mixing states of Amazon basin aerosol particles transported over long distances using transmission electron microscopy, Atmos. Chem. Phys., 20, 11923-11939, https://doi.org/10.5194/acp-20-11923-2020, 2020.

Amil, N., Latif, M. T., Khan, M. F., and Mohamad, M.: Seasonal variability of PM2.5 composition and sources in the Klang Valley urban-industrial environment, Atmos. Chem. Phys., 16, 5357-5381, https://doi.org/10.5194/acp-16-5357-2016, 2016.

Andreae, M. O., Charlson, R. J., Bruynseels, F., Storms, H., Grieken, R. Van, and Maenhaut, W.: Internal mixture of sea salt, silicates, and excess sulfate in marine aerosols, Science, 232(4758), 1620-1623, https://doi.org/10.1126/science.232.4758.1620, 1986.

Angle, K. J., Crocker, D. R., Simpson, R. M. C., Mayer, J. J., Garofalo, L. A., Moore, A. N., Mora Garcia, S. L., Or, V. W., Srinivasan, S., Farhan, M., Sauer, J. S., Lee, C., Pothier, M. A., Farmer, D. K., Martz, T. R., Bertram, T. H., Cappa, C. D., Prather, K. A., and Grassian, V. H.: Acidity across the interface from the ocean surface to sea spray aerosol, P. Natl. Acad. Sci. USA, 118, e2018397118, https://doi.org/10.1073/pnas.2018397118, 2021.

Baker, A. R., and Jickells, T. D.: Mineral particle size as a control on aerosol iron solubility. Geophys. Res. Lett., 33, L17608. https://doi.org/10.1029/2006GL026557, 2006.

Baker, A. R., Jickells, T. D., Witt, M., and Linge, K. L.: Trends in the solubility of iron, aluminium, manganese and phosphorus in aerosol collected over the Atlantic Ocean, Mar. Chem., 98, 43-58, https://doi.org/10.1016/j.marchem.2005.06.004, 2006.

Bie, S., Yang, L., Zhang, Y., Huang, Q., Li, J., Zhao, T., Zhang, X., Wang, P., and Wang, W.: Source appointment of PM2.5 in Qingdao Port, East of China, Sci. Total. Environ., 755, https://doi.org/10.1016/j.scitotenv.2020.142456, 2021.

Borai, E. H., El-Sofany, E. A., Abdel-Halim, A. S., and Soliman, A. A.: Speciation of hexavalent chromium in atmospheric particulate samples by selective extraction and ion chromatographic determination, Trac-Trend. Anal. Chem., 21, 741-745, https://doi.org/10.1016/S0165-9936(02)01102-0, 2002.

Boyd, P. W., Watson, A. J., Law, C. S., Abraham, E. R., Trull, T., Murdoch, R., Bakker, D. C. E., Bowie, A. R., Buesseler, K. O., Chang, H., Charette, M., Croot, P., Downing, K., Frew, R., Gall, M., Hadfield, M., Hall, J., Harvey, M., Jameson, G., LaRoche, J., Liddicoat, M., Ling, R., Maldonado, M. T., McKay, R. M., Nodder, S., Pickmere, S., Pridmore, R., Rintoul, S., Safi, K., Sutton, P., Strzepek, R., Tanneberger, K., Turner, S., Waite, A., and Zeldis, J.: A mesoscale phytoplankton bloom in the polar Southern Ocean stimulated by iron fertilization, Nature, 407, 695-702, https://doi.org/10.1038/35037500, 2000.

Buck, C. S., Landing, W. M., and Resing, J. A.: Particle size and aerosol iron solubility: A high-resolution analysis of Atlantic aerosols, Mar. Chem., 120, 14-24, https://doi.org/10.1016/j.marchem.2008.11.002, 2010.

Chang, Y., Huang, K., Xie, M., Deng, C., Zou, Z., Liu, S., and Zhang, Y.: First long-term and near real-time measurement of trace elements in China's urban atmosphere: Temporal variability, source apportionment and precipitation effect. Atmos. Chem. Phys., 18, 11793-11812. https://doi.org/10.5194/acp-18-11793-2018, 2018.

Chen, J., Liu, G., Kang, Y., Wu, B., Sun, R. Y., Zhou, C. C., and Wu., D.: Atmospheric emissions of F, As, Se, Hg, and Sb from coal-fired power and heat generation in China, Chemosphere, 90, 1925-1932, http://doi.org/10.1016/j.chemosphere.2012.10.032, 2013.

Chen, J., Tan, M., Li, Y., Zheng, J., Zhang, Y., Shan, Z., Zhang, G., and Li, Y.: Characteristics of trace elements and lead isotope ratios in PM2.5 from four sites in Shanghai, J. Hazard. Mater., 156, 36-43, https://doi.org/10.1016/j.jhazmat.2007.11.122, 2008.

Choobari, O. A., Zawar-Reza, P., and Sturman, A.: The global distribution of mineral dust and its impacts on the climate system: A review, Atmos. Res., 138, 152-165, https://doi.org/10.1016/j.atmosres.2013.11.007, 2014.

Draxler, R. R., and Rolph, G. D.: HYSPLIT (HYbrid Single-Particle Lagrangian Integrated Trajectory) Model access via NOAA ARL READY Website, last, NOAA Air Resources Laboratory, College Park, MD, 2014.

Desboeufs, K. V., Losno, R., Vimeux, F., and Cholbi, S.: The pH‐dependent dissolution of wind‐transported Saharan dust, J. Geophys. Res., 104, 21,287–21,299, https://doi.org/10.1029/1999JD900236, 1999.

Falkowski, P. G., Barber, R. T., and Smetacek, V.: Biogeochemical controls and feedbacks on ocean primary production, Science, 281, 200-206, https://doi.org/10.1126/science.281.5374.200, 1998.

Feng, L., Shen, H., Zhu, Y., Gao, H., and Yao, X.: Insight into Generation and Evolution of Sea-Salt Aerosols from Field Measurements in Diversified Marine and Coastal Atmospheres, Sci. Rep., 7, 41260, https://doi.org/10.1038/srep41260, 2017.

Gen, M., Zhang, R., and Chen, C. K.: Nitrite/Nitrous Acid Generation from the Reaction of Nitrate and Fe(II) Promoted by Photolysis of Iron-Organic Complexes. Environ. Sci. Technol., 55, 15715-15723. https://doi.org/ 10.1021/acs.est.1c05641, 2022.

Geng, H., Hwang, H., Liu, X., Dong, S., and Ro, C. U.: Investigation of aged aerosols in size-resolved Asian dust storm particles transported from Beijing, China, to Incheon, Korea, using low-Z particle EPMA. Atmos. Chem. Phys., 14, 3307-3323. https://doi.org/10.5194/acp-14-3307-2014. 2014.

Gu, J., Pitz, M., Schnelle-Kreis, J., Diemer, J., Reller, A., Zimmermann, R., Soentgen, J., Stoelzel, M., Wichmann, H.-E., Peters, A., and Cyrys, J.: Source apportionment of ambient particles: Comparison of positive matrix factorization analysis applied to particle size distribution and chemical composition data, Atmos. Environ., 45, 1849-1857, https://doi.org/10.1016/j.atmosenv.2011.01.009, 2011.

Gugamsetty, B., Wei, H., Liu, C. N., Awasthi, A., Hsu, S. C., Tsai, C. J., Roam, G. D., Wu, Y. C., and Chen, C. F.: Source Characterization and Apportionment of PM10, PM2.5 and PM0.1 by Using Positive Matrix Factorization, Aerosol Air Qual. Res., 12, 476-491, https://doi.org/10.4209/aaqr.2012.04.0084, 2012.

Hawco, N. J., Tagliabue, A. and Twining, B. S.: Manganese limitation of phytoplankton physiology and productivity in the Southern Ocean. Global Biogeochem. Cycles, 36, e2022GB007382. https://doi.org/10.1029/2022GB007382, 2022.

Hilario, M. R. A., Cruz, M. T., Cambaliza, M. O. L., Reid, J. S., Xian, P., Simpas, J. B., Lagrosas, N. D., Uy, S. N. Y., Cliff, S., and Zhao, Y.: Investigating size-segregated sources of elemental composition of particulate matter in the South China Sea during the 2011 Vasco cruise, Atmos. Chem. Phys., 20, 1255-1276, https://doi.org/10.5194/acp-20-1255-2020, 2020.

Ho, K. F., Lee, S. C., Chow, J. C., and Watson, J. G.: Characterization of PM10 and PM2.5 source profiles for fugitive dust in Hong Kong, Atmos. Environ., 37, 1023-1032, https://doi.org/10.1016/S1352-2310(02)01028-2, 2003.

Hsieh, C. -C., Chen, H. -Y., & Ho, T. -Y.: The effect of aerosol size on Fe solubility and deposition flux: A case study in the East China Sea, Mar. Chem., 241, 104106, https://doi.org/10.1016/j.marchem.2022.104106, 2022.

Hsieh, C. -C., You, C. -F., & Ho, T. -Y.: The solubility and deposition flux of East Asian aerosol metals in the East China Sea: The effects of aeolian transport processes, Mar. Chem., 253, 104268, https://doi.org/10.1016/j.marchem.2023.104268, 2023.

Hsu, S.-C., Liu, S. C., Arimoto, R., Shiah, F.-K., Gong, G.-C., Huang, Y.-T., Kao, S.-J., Chen, J.-P., Lin, F.-J., Lin, C.-Y., Huang, J.-C., Tsai, F., and Lung, S.-C. C.: Effects of acidic processing, transport history, and dust and sea salt loadings on the dissolution of iron from Asian dust, J. Geophys. Res.-Atmos., 115, D19313. https://doi.org/10.1029/2009JD013442, 2010a.

Hsu, S. C., Wong, G. T. F., Gong, G. C., Shiah, F. K., Huang, Y. T., Kao, S. J., Tsai, F. J., Lung, S. C. C., Lin, F. J., Lin, II, Hung, C. C., and Tseng, C. M.: Sources, solubility, and dry deposition of aerosol trace elements over the East China Sea, Mar. Chem., 120, 116-127, https://doi.org/10.1016/j.marchem.2008.10.003, 2010b.

Hsu, S. -C., Liu, S. C., Kao, S. J., Jeng, W. L., Huang, Y. T., Tseng, C. M., Tsai, F., Tu, J. Y., and Yang, T.: Water‐soluble species in the marine aerosol from the northern South China Sea: High chloride depletion related to air pollution, J. Geophys. Res., 112, D19304, https://doi.org/10.1029/2007JD008844, 2007.

Huang, J., Wang, T., Wang, W., Li, Z., and Yan, H.: Climate effects of dust aerosols over East Asian arid and semiarid regions, J. Geophys. Res.-Atmos., 119, 11398-11416, https://doi.org/10.1002/2014JD021796, 2014.

Ito, A. and Feng, Y.: Iron mobilization in North African Dust, Earth System Science 2010: Global Change, Climate and People, WOS:000312268000004, https://doi.org/10.1016/j.proenv.2011.05.004, 2011.

Ito, A., Ye, Y., Baldo, C., and Shi, Z. B.: Ocean fertilization by pyrogenic aerosol iron. npj Clim. Atmos. Sci., 4, Article 30. https://doi.org/10.1038/s41612-021-00185-8, 2021.

Jickells, T. D., An, Z. S., Andersen, K. K., Baker, A. R., Bergametti, G., Brooks, N., Cao, J. J., Boyd, P. W., Duce, R. A., Hunter, K. A., Kawahata, H., Kubilay, N., laRoche, J., Liss, P. S., Mahowald, N., Prospero, J. M., Ridgwell, A. J., Tegen, I., and Torres, R.: Global iron connections between desert dust, ocean biogeochemistry, and climate, Science, 308, 67-71, https://doi.org/10.1126/science.1105959, 2005.

Karar, K., Gupta, A. K., Kumar, A., and Biswas, A. K.: Characterization and identification of the sources of chromium, zinc, lead, cadmium, nickel, manganese and iron in Pm-10 particulates at the two sites of kolkata, india, Environ. Monit. Assess., 120, 347-360, https://doi.org/10.1007/s10661-005-9067-7, 2006.

Kim, N., Yum, S. S., Cho, S., Jung, J., Lee, G., and Kim, H.: Atmospheric sulfate formation in the Seoul Metropolitan Area during spring/summer: Effect of trace metal ions. Environ. Pollut., 315, 120379. https://doi.org/10.1016/j.envpol.2022.120379, 2022.

Knopf, D. A., Charnawskas, J. C., Wang, P., Wong, B., Tomlin, J. M., Jankowski, K. A., Fraund, M., Veghte, D. P., China, S., Laskin, A., Moffet, R. C., Gilles, M. K., Aller, J. Y., Marcus, M. A., Raveh-Rubin, S., and Wang, J.: Micro-spectroscopic and freezing characterization of ice-nucleating particles collected in the marine boundary layer in the eastern North Atlantic, Atmos. Chem. Phys., 22, 5377–5398, https://doi.org/10.5194/acp-22-5377-2022, 2022.

Kwak, N., Lee, H., Maeng, H., Seo, A., Lee, K., Kim, S., Lee, M., Cha, J. W., Shin, B., and Park, K.: Morphological and chemical classification of fine particles over the Yellow Sea during spring, 2015–2018, Environ. Pollut., 305, 119286, https://doi.org/10.1016/j.envpol.2022.119286, 2022.

Lee, J. H., Hopke, P. K., and Turner, J. R.: Source identification of airborne PM2.5 at the St. Louis-Midwest Supersite, J. Geophys. Res.-Atmos., 111, https://doi.org/10.1029/2005JD006329, 2006.

Li, P., Li, Q., Shi, J., Gao, H., and Yao, X.: Concentration, solubility, and dry deposition flux of trace elements in fine and coarse particles in Qingdao during summer (in Chinese), Environ. Sci., 39, 3067-3074, https://doi.org/10.13227/j.hjkx.201712231, 2018.

Li, Q., Cheng, H., Zhou, T., Lin, C., and Guo, S.: The estimated atmospheric lead emissions in China, 1990-2009, Atmos. Environ., 60, 1-8, https://doi.org/10.1016/j.atmosenv.2012.06.025, 2012.

Li, R., Wang, Q., He, X., Zhu, S., Zhang, K., Duan, Y., Fu, Q., Qiao, L., Wang, Y., Huang, L., Li, L., and Yu, J. Z.: Source apportionment of PM2.5 in Shanghai based on hourly organic molecular markers and other source tracers, Atmos. Chem. Phys., 20, 12047-12061, https://doi.org/10.5194/acp-20-12047-2020, 2020.

Li, T., Wang, Y., Li, W., Chen, J., Wang, T., and Wang, W.: Concentrations and solubility of trace elements in fine particles at a mountain site, southern China: regional sources and cloud processing, Atmos. Chem. Phys., 15, 8987-9002, https://doi.org/10.5194/acp-15-8987-2015, 2015.

Li, T., Wang, Y., Zhou, J., Wang, T., Ding, A., Nie, W., Xue, L., Wang, X., and Wang, W.: Evolution of trace elements in the planetary boundary layer in southern China: Effects of dust storms and aerosol-cloud interactions, J. Geophys. Res.-Atmos., 122, 3492-3506, https://doi.org/10.1002/2016JD025541, 2017.

Li, W., Qi, Y., Liu, Y., Wu, G., Zhang, Y., Shi, J., Qu, W., Sheng, L., Wang, W., Zhang, D., and Zhou, Y.: Daytime and nighttime aerosol soluble iron formation in clean and slightly polluted moist air in a coastal city in eastern China, Atmos. Chem. Phys., 24, 6495-6508, https://doi.org/10.5194/acp-24-6495-2024, 2024.

Li, W., Qi, Y., Qu, W., Qu, W., Shi, J., Zhang, D., Liu, Y., Wu, F., Ma, Y., Zhang, Y., Ren, D., Du, X., Yang, S., Wang, X., Yi, L., Gao, X., Wang, W., Ma, Y., Sheng, L., and Zhou, Y.: Sulfate and nitrate elevation in reverse-transport dust plumes over coastal areas of China, Atmos. Environ., 295, 119518, Article 119518. https://doi.org/10.1016/j.atmosenv.2022.119518, 2023.

Li, W., Qi, W., Wu, G., Zhang, Y., Han, R., Liu, Y., Qu, W., Song, Y., Wang, X., Chen, T., Sheng, L., Shi, J., Zhang, D., and Zhou, Y.: Anthropogenic dominance and secondary processes drive aerosol iron solubility in Asian continental outflow: insights from spring Qingdao, China, Environ. Sci. Technol. Air, 2, 1840-1848, https://doi.org/10.1021/acsestair.5c00049, 2025.

Li, W., Wang, W., Zhou, Y., Ma, Y., Zhang, D., and Sheng, L.: Occurrence and Reverse Transport of Severe Dust Storms Associated with Synoptic Weather in East Asia, Atmosphere, 10, https://doi.org/10.3390/atmos10010004, 2019.

Li, X., Wang, S, Duan, L., Hao, J., Li, C., Chen, Y., and Yang, L.: Particulate and trace gas emissions from open burning of wheat straw and corn stover in China. Environ. Sci. Technol. 41, 6052-6058, https://doi.org/10.1021/es0705137, 2007.

Li, Y.-X., Luo, L., Li, J.-W., Hsu, S.-C, Ni, Y.-Z., and Kao, S.-J.: Middle East and Central Asian dust reaches the South China Sea in summer. Natl. Sci. Rev., nwaf274. https://doi.org/10.1093/nsr/nwaf274, 2025.

Li, Z., Ho, K.-F., Dong, G., Lee, H. F., and Yim, S. H. L.: A novel approach for assessing the spatiotemporal trend of health risk from ambient particulate matter components: Case of Hong Kong. Environ. Res., 204, 111866. https://doi.org/10.1016/j.envres.2021.111866, 2022.

Lin, Y.-C., Yu, M., Xie, F., and Zhang, Y. Anthropogenic Emission Sources of Sulfate Aerosols in Hangzhou, East China: Insights from Isotope Techniques with Consideration of Fractionation Effects between Gas-to-Particle Transformations. Environ. Sci. Technol., 56, 3905-3914. https://doi.org/10.1021/acs.est.1c05823, 2022.

Liu, B., Song, N., Dai, Q., Mei, R., Sui, B., Bi, X., and Feng, Y.: Chemical composition and source apportionment of ambient PM2.5 during the non-heating period in Taian, China, Atmos. Res., 170, 23-33, https://doi.org/10.1016/j.atmosres.2015.11.002, 2016.

Liu, B., Sun, X., Zhang, J., Bi, X., Li, Y., Li, L., Dong, H., Xiao, Z., Zhang, Y., and Feng, Y.: Characterization and Spatial Source Apportionments of Ambient PM10 and PM2.5 during the Heating Period in Tian'jin, China, Aerosol Air Qual. Res., 20, 1-13, https://doi.org/10.4209/aaqr.2019.06.0281, 2020.

Liu, X., Zhang, X., Jin, B., Wang, T., Qian, S., Zou, J., Dinh, V. N. T., Jaffrezo, J. -L., Uzu, G., Dominutti, P., Darfeuil, S., Fzvez, O., Conil, S., Marchand, N., Castillo, S., de la Rosa, J., Grange, S., Hueglin, C., Eleftheriadis, K., Diapouli, E., Manousakas, M. -I., Gini, M., Nava, S., Calzolai, G., Alves, C., Monge, M., Reche, C., Harrison, R. M., Hopke, P. K., Alastuey, A., and Querol, X.: Source apportionment of PM_{10} based on offline chemical speciation data at 24 European sites, npj Clim. Atmos. Sci., 8, 255, https://doi.org/10.1038/s41612-025-01097-7, 2025.

López-García, P., Gelado-Caballero, M. D., Collado-Sánchez, C., and Hernández-Brito, J. J.: Solubility of aerosol trace elements: Sources and deposition fluxes in the Canary Region, Atmos. Environ., 148, 167-174, https://doi.org/10.1016/j.atmosenv.2016.10.035, 2017.

Luo, C., Mahowald, N., Bond, T., Chuang, P. Y., Artaxo, P., Siefert, R., Chen, Y., and Schauer, J.: Combustion iron distribution and deposition, Global Biogeochem. Cy., 22, https://doi.org/10.1029/2007GB002964, 2008.

Luo, C. H., Wang, W. C., Sheng, L. F., Zhou, Y., Hu, Z. Y., Qu, W. J., Li, X. D., and Hai, S. F.: Influence of polluted dust on chlorophyll-a concentration and particulate organic carbon in the subarctic North Pacific Ocean based on satellite observation and the WRF-Chem simulation, Atmos. Res., 236, 104812, https://doi.org/10.1016/j.atmosres.2019.104812, 2020.

Ma, Y. N., Ma, Y. J., Zhang, X. G., Wu, F. K., Liu, Q., Wu, X. Y., Lyu, Y., Jiang, J. W., Zhao, D. D., Ren, X. B., Li, Z., Jia, X., Li, M. C., Yao, J. Y., Gao, Z. M., Hai, S. F., and Xin, J. Y.: Shipboard Observations of Aerosol Chemical Properties Over the Western Pacific Ocean in Winter 2018. J. Geophys. Res.-Atmos., 128, Article e2023JD039422. https://doi.org/10.1029/2023JD039422, 2023.

Mackey, K. R. M., Buck, K. N., Casey, J. R., Cid, A., Lomas, M. W., Sohrin, Y., and Paytan, A.: Phytoplankton responses to atmospheric metal deposition in the coastal and open-ocean Sargasso Sea. Front. Microbiol., 3, https://doi.org/10.3389/fmicb.2012.00359, 2012.

Mahowald, N.: Aerosol Indirect Effect on Biogeochemical Cycles and Climate, Science, 334, 794-796, https://doi.org/10.1126/science.1207374, 2011.

Mann, E. L., Ahlgren, N., Moffett, J. W., and Chisholm, S. W.: Copper toxicity and cyanobacteria ecology in the Sargasso Sea, Limnol. Oceanogr., 47, 976-988, https://doi.org/10.4319/lo.2002.47.4.0976, 2002.

Martin, J. H.: Glacial-interglacial CO2 change: The iron hypothesis, Paleoceanography, 5, 1-13, https://doi.org/10.1029/PA005i001p00001, 1990.

Meng, Y., Li, P., Cao, W., Shi, J., Gao, H., and Yao, X.: Size distribution of particulate trace elements in mass concentration and their size-dependent solubility in the atmosphere in Qingdao, China (in Chinese), China Environ. Sci., 37, 851-858, 2017.

Ming, L., Jin, L., Li, J., Fu, P., Yang, W., Liu, D., Zhang, G., Wang, Z., and Li, X.: PM2.5 in the Yangtze River Delta, China: Chemical compositions, seasonal variations, and regional pollution events. Environ. Pollut., 223, 200-212. https://doi.org/10.1016/j.envpol.2017.01.013, 2017.

Morel, F. M. M. and Price, N. M.: The biogeochemical cycles of trace metals in the oceans, Science, 300, 944-947, https://doi.org/10.1126/science.1083545, 2003.

Mustaffa, N. I. H., Latif, M. T., Ali, M. M., and Khan, M. F.: Source apportionment of surfactants in marine aerosols at different locations along the Malacca Straits, Environ. Sci. Pollut. R., 21, 6590-6602, https://doi.org/10.1007/s11356-014-2562-z, 2014.

Nagajyoti, P. C., Lee, K. D., and Sreekanth, T. V. M.: Heavy metals, occurrence and toxicity for plants: a review. Environ. Chem. Lett., 8, 199-216. https://doi.org/10.1007/s10311-010-0297-8, 2010.

Norris, G., Duvall, R., Brown, S., and Bai, S.: EPA positive matrix factorization (PMF) 5.0 fundamentals and user guide, US Environmental Protection Agency Office of Research and Development, Washington, DC, https://www.epa.gov/air-research/epa-positive-matrix-factorization-50-fundamentals-and-user-guide, 2014.

Okada, K., Naruse, H., Tanaka, T., Nemoto, O., Iwasaka, Y., Wu, P. -M., Ono, A., Duce, R. A., Uematsu, M., Merrill, J. T., and Arao, K.: X-ray spectrometry of individual Asian dust-storm particles over the Japanese islands and the North Pacific Ocean, Atmos. Environ., 24(6), 1369-1378, https://doi.org/10.1016/0960-1686(90)90043-M, 1990.

Paatero, P. and Tapper, U.: Positive matrix factorization - a nonnegative factor model with optimal utilization of error-estimates of data values, Environmetrics, 5, 111-126, https://doi.org/10.1002/env.3170050203, 1994.

Pant, P. and Harrison, R. M.: Estimation of the contribution of road traffic emissions to particulate matter concentrations from field measurements: A review, Atmos. Environ., 77, 78-97, https://doi.org/10.1016/j.atmosenv.2013.04.028, 2013.

Peng, L., Cui, X., Wang, X., Guo, Y., Ma, Y., Wen, Y., Wang, Z., Guo, Y., and Sun, J. Occurrence, source, and ecological impacts of dry depositing aerosol metal elements in the Bohai Bay. Mar. Environ. Res., 208, 107137, https://doi.org/10.1016/j.marenvres.2025.107137, 2025.

Pey, J., Alastuey, A., and Querol, X.: PM_{10} and $PM_{2.5}$ sources at an insular location in the western Mediterranean by using source apportionment techniques, Sci. Total. Environ., 456-457, 267-277, http://dx.doi.org/10.1016/j.scitotenv.2013.03.084, 2013.

Polissar, A. V., Hopke, P. K., and Poirot, R. L.: Atmospheric aerosol over Vermont: Chemical composition and sources, Environ. Sci. Technol., 35, 4604-4621, https://doi.org/10.1021/es0105865, 2001.

Prijith, S. S., Aloysius, M., and Mohan, M.: Relationship between wind speed and sea salt aerosol production: A new approach, J. Atmos. Sol.-Terr. Phy., 108, 34-40, https://doi.org/10.1016/j.jastp.2013.12.009, 2014.

Qi, Y. and Zhou, Y.: A review of the iron and its solubility in atmospheric aerosols (in Chinese), J. Mar. Meteorol., 41, 1-13, https://doi.org/10.19513/j.cnki.issn2096-3599.2021.02.001, 2021.

Qiu, S.: Solubility of iron in atmospheric aerosols and related factors in Marginal Seas, China (in Chinese), M.S. Thesis, Ocean University of China, Qingdao, China, 2015.

Rai, P., Chakraborty, A., Mandariya, A. K., and Gupta, T.: Composition and source apportionment of PM1 at urban site Kanpur in India using PMF coupled with CBPF, Atmos. Res., 178, 506-520, https://doi.org/10.1016/j.atmosres.2016.04.015, 2016.

Ramanathan, V., Ramana, M. V., Roberts, G., Kim, D., Corrigan, C., Chung, C., and Winker, D.: Warming trends in Asia amplified by brown cloud solar absorption, Nature, 448, 575-U575, https://doi.org/10.1038/nature06019, 2007.

Sakata, K., Kurisu, M., Takeichi, Y., Sakaguchi, A., Tanimoto, H., Tamenori, Y., Matsuki, A., and Takahashi, Y.: Iron (Fe) speciation in size-fractionated aerosol particles in the Pacific Ocean: The role of organic complexation of Fe with humic-like substances in controlling Fe solubility, Atmos. Chem. Phys., 22, 9461-9482, https://doi.org/10.5194/acp-22-9461-2022, 2022.

Schroth, A. W., Crusius, J., Sholkovitz, E. R., and Bostick, B. C.: Iron solubility driven by speciation in dust sources to the ocean, Nat. Geosci., 2, 337-340, https://doi.org/10.1038/NGEO501, 2009.

Sharma, S. K., Sharma, A., Saxena, M., Choudhary, N., Masiwal, R., Mandal, T. K., and Sharma, C.: Chemical characterization and source apportionment of aerosol at an urban area of Central Delhi, India, Atmos. Pollut. Res., 7, 110-121, https://doi.org/10.1016/j.apr.2015.08.002, 2016.

Shelley, R. U., Morton, P. L., and Landing, W. M.: Elemental ratios and enrichment factors in aerosols from the US-GEOTRMES North Atlantic transects, Deep-Sea Res. Pt. II, 116, 262-272, https://doi.org/10.1016/j.dsr2.2014.12.005, 2015.

Shi, J.-H., Gao, H.-W., Zhang, J., Tan, S.-C., Ren, J.-L., Liu, C.-G., Liu, Y., and Yao, X.: Examination of causative link between a spring bloom and dry/wetdeposition of Asian dust in the Yellow Sea, China, J. Geophys. Res.-Atmos., 117, D17394, https://doi.org/10.1029/2012JD017983, 2012.

Shi, J.-H., Zhang, J., Gao, H.-W., Tan, S.-C., Yao, X.-H., and Ren, J.-L.: Concentration, solubility and deposition flux of atmospheric particulate nutrients over the Yellow Sea, Deep-Sea Res. Pt. II, 97, 43-50, https://doi.org/10.1016/j.dsr2.2013.05.004, 2013.

Shi, Z., Krom, M. D., Jickells, T. D., Bonneville, S., Carslaw, K. S., Mihalopoulos, N., Baker, A. R., and Benning, L. G.: Impacts on iron solubility in the mineral dust by processes in the source region and the atmosphere: A review, Aeolian Res., 5, 21-42, https://doi.org/10.1016/j.aeolia.2012.03.001, 2012.

Sholkovitz, E. R., Sedwick, P. N., Church, T. M., Baker, A. R., and Powell, C. F.: Fractional solubility of aerosol iron: Synthesis of a global-scale data set, Geochim. Cosmochim. Ac., 89, 173-189, https://doi.org/10.1016/j.gca.2012.04.022, 2012.

Sorooshian, A., Wang, Z., Coggon, M. M., Jonsson, H. H., and Ervens, B.: Observations of Sharp Oxalate Reductions in Stratocumulus Clouds at Variable Altitudes: Organic Acid and Metal Measurements During the 2011 E-PEACE Campaign, Environ. Sci. Technol., 47, 7747-7756, https://doi.org/10.1021/es4012383, 2013.

Spokes, L. J., and Jickells, T. D.: Factors controlling the solubility of aerosol trace metals in the atmosphere and on mixing into seawater, Aquat. Geochem., 1, 355–374, https://doi.org/10.1007/BF00702739, 1996.

Sun. H., Sun, J., Zhu, C., Yu, L., Lou, Y., Li, R., and Lin, Z.: Chemical characterizations and sources of PM2.5 over the offshore Eastern China sea: Water soluble ions, stable isotopic compositions, and metal elements. Atmos. Pollut. Res., 13, 101410. https://doi.org/10.1016/j.apr.2022.101410, 2022.

Sun, M., Qi, Y., Li, W., Zhu, W., Yang, Y., Wu, G., Zhang, Y., Zhao, Y., Shi, J., Sheng, L., Wang, W., Liu, Y., Qu, W., Wang, X., and Zhou, Y. Investigation of a haze-to-dust and dust swing process at a coastal city in northern China part II: A study on the solubility of iron and manganese across aerosol sources and secondary processes. Atmos. Environ., 328, 120532. https://doi.org/10.1016/j.atmosenv.2024.120532, 2024.

Tang, W. Y., Llort, J., Weis, J., Perron, M. M. G., Basart, S., Li, Z. C., Sathyendranath, S., Jackson, T., Rodriguez, E. S., Proemse, B. C., Bowie, A. R., Schallenberg, C., Strutton, P. G., Matear, R., and Cassar, N.: Widespread phytoplankton blooms triggered by 2019-2020 Australian wildfires, Nature, 597, 370-375, https://doi.org/10.1038/s41586-021-03805-8, 2021.

Taylor, S. R.: Trace element abundances and the chondritic earth model, Geochim. Cosmochim. Ac., 28, 1989-1998, https://doi.org/10.1016/0016-7037(64)90142-5, 1964.

Tian, H., Cheng, K., Wang, Y., Zhao, D., Lu, L., Jia, W., and Hao, J.: Temporal and spatial variation characteristics of atmospheric emissions of Cd, Cr, and Pb from coal in China, Atmos. Environ., 50, 157-163, https://doi.org/10.1016/j.atmosenv.2011.12.045, 2012.

Tian, H., Liu, K., Zhou, J., Lu, L., Hao, J., Qiu, P., Gao, J., Zhu, C., Wang, K., and Hua, S.: Atmospheric Emission Inventory of Hazardous Trace Elements from China's Coal-Fired Power Plants-Temporal Trends and Spatial Variation Characteristics, Environ. Sci. Technol., 48, 3575-3582, http://doi.org/10.1021/es404730j, 2014.

van Pinxteren, D., Brüggemann, E., Gnauk, T., Müller, K., Thiel, C., and Herrmann, H.: A GIS based approach to back trajectory analysis for the source apportionment of aerosol constituents and its first application, J. Atmos. Chem., 67, 1-28, https://doi.org/10.1007/s10874-011-9199-9, 2010.

Vu, T. V., Delgado-Saborit, J. M., and Harrison, R. M.: Review: Particle number size distributions from seven major sources and implications for source apportionment studies, Atmos. Environ., 122, 114-132, https://doi.org/10.1016/j.atmosenv.2015.09.027, 2015.

Wagener, T., Guieu, C., Losno, R., Bonnet, S., and Mahowald, N.: Revisiting atmospheric dust export to the Southern Hemisphere ocean: Biogeochemical implications, Global Biogeochem. Cycles, 22, GB2006, https://doi.org/10.1029/2007GB002984, 2008.

Wang, L., Qi, J. H., Shi, J. H., Chen, X. J., and Gao, H. W.: Source apportionment of particulate pollutants in the atmosphere over the Northern Yellow Sea, Atmos. Environ., 70, 425-434, https://doi.org/10.1016/j.atmosenv.2012.12.041, 2013.

Wang, Q., Qiao, L., Zhou, M., Zhu, S., Griffith, S., Li, L., and Yu, J. Z.: Source Apportionment of PM2.5 Using Hourly Measurements of Elemental Tracers and Major Constituents in an Urban Environment: Investigation of Time-Resolution Influence, J. Geophys. Res.-Atmos., 123, 5284-5300, https://doi.org/10.1029/2017JD027877, 2018.

Wang, W., Luo, C., Sheng, L., Zhao, C., Zhou, Y., and Chen, Y.: Effects of biomass burning on chlorophyll-a concentration and particulate organic carbon in the subarctic North Pacific Ocean based on satellite observations and WRF-Chem model simulations: A case study, Atmos. Res., 254, 105526, https://doi.org/doi.org/10.1016/j.atmosres.2021.105526, 2021.

Wang, W. C., He, Z. Z., Hai, S. F., Sheng, L. F., Han, Y. Q., and Zhou, Y.: Dust Aerosol's Deposition and its Effects on Chlorophyll-A Concentrations Based on Multi-Sensor Satellite Observations and Model Simulations: A Case Study, Front. Env. Sci.-Switz., 10, 875365, https://doi.org/10.3389/fenvs.2022.875365, 2022.

Wang, Y., Cheng, K., Tian, H.-Z., Yi, P., and Xue, Z.-G.: Emission Characteristics and Control Prospects of Primary PM2.5 from Fossil Fuel Power Plants in China, Aerosol Air Qual. Res., 16, 3290-3301, http://doi.org/10.4209/aaqr.2016.07.0324, 2016.

Wu, C., Huang, X. H. H., Ng, W. M., Griffith, S. M., and Yu, J. Z.: Inter-comparison of NIOSH and IMPROVE protocols for OC and EC determination: implications for inter-protocol data conversion, Atmos. Meas. Tech., 9, 4547-4560, https://doi.org/10.5194/amt-9-4547-2016, 2016.

Wu, H. Y., Hsieh, C. C., and Ho, T. Y.: Trace metal dissolution kinetics of East Asian size-fractionated aerosols in seawater: The effect of a model siderophore, Mar. Chem., 254, 104277, https://doi.org/10.1016/j.marchem.2023.104277, 2023.

Wu, R., Zhou, X., Wang, L., Wang, Z., Zhou, Y., Zhang, J., and Wang, W.: PM2.5 Characteristics in Qingdao and across Coastal Cities in China, Atmosphere, 8, https://doi.org/10.3390/atmos8040077, 2017.

Wu, S. P., Cai, M. J., Xu, C., Zhang, N., Zhou, J. B., Yan, J. P., Schwab, J. J., and Yuan, C. S.: Chemical nature of PM2.5 and PM10 in the coastal urban Xiamen, China: Insights into the impacts of shipping emissions and health risk, Atmos. Environ., 227, https://doi.org/10.1016/j.atmosenv.2020.117383, 2020.

Xu, B., Xu, H., Zhao, H., Gao, J., Liang, D., Li, Y., Wang, W., Feng, Y., and Shi, G.: Source apportionment of fine particulate matter at a megacity in China, using an improved regularization supervised PMF model. Sci. Total Environ., 879, 163198. https://doi.org/10.1016/j.scitotenv.2023.163198, 2023.

Xu, L., Liu, X. H., Gao, H. W., Yao, X. H., Zhang, D. Z., Bi, L., Liu, L., Zhang, J., Zhang, Y. X., Wang, Y. Y., Yuan, Q., and Li, W. J.: Long-range transport of anthropogenic air pollutants into the marine air: insight into fine particle transport and chloride depletion on sea salts. Atmos. Chem. Phys., 21, 17715-17726. https://doi.org/10.5194/acp-21-17715-2021, 2021.

Xu, L., Zhi, M. K., Liu, X. H., Gao, H. W., Yao, X. H., Yuan, Q., Fu, P. Q., and Li, W. J.: Direct evidence of pyrogenic aerosol iron by intrusions of continental polluted air into the Eastern China Seas, Atmos. Res., 292, 106839, https://doi.org/10.1016/j.atmosres.2023.106839, 2023.

Yang, F., Tan, J., Zhao, Q., Du, Z., He, K., Ma, Y., Duan, F., Chen, G., and Zhao, Q.: Characteristics of PM2.5 speciation in representative megacities and across China, Atmos. Chem. Phys., 11, 5207-5219, https://doi.org/10.5194/acp-11-5207-2011, 2011.

Yang, T., Chen, Y., Zhou, S., Li, H., Wang, F., and Zhu, Y.: Solubilities and deposition fluxes of atmospheric Fe and Cu over the Northwest Pacific and its marginal seas, Atmos. Environ., 239, 117763, https://doi.org/10.1016/j.atmosenv.2020.117763, 2020.

Yang, X., Zheng, M., Liu, Y., Yan, C., Liu, J., Liu, J., and Cheng, Y.: Exploring sources and health risks of metals in Beijing PM2.5: Insights from long-term online measurements. Sci. Total Environ., 814, 151954. https://doi.org/10.1016/j.scitotenv.2021.151954, 2022.

Yang, Y., Sun, M., Wu, G., Qi, Y., Zhu, W., Zhao, Y., Zhu, Y., Li, W., Zhang, Y., Wang, N., Sheng, L., Wang, W., Yu, X., Yen, P. -H., Yuan, C. -S., Ceng, J. -H., Chiang, K. -C., Tseng, Y. -L., Soong, K. -Y., and Jeng, M. -S.: Inter-comparison of chemical fingerprint and source apportionment of marine fine particles at two islands through the west and east passages of the Taiwan Island. Sci. Total Environ., 851, 158313. http://dx.doi.org/10.1016/j.scitotenv.2022.158313, 2022a.

Yen, P. -H., Yuan, C. -S., Wu, C. -H., Yeh, M. -J., Tseng, Y. -L., Soong, K. -Y.: Transport route-based cluster analysis of chemical fingerprints and source origins of marine fine particles (PM2.5) in South China Sea. Sci. Total Environ., 806, 150591. https://doi.org/10.1016/j.scitotenv.2021.150591, 2022b.

Yoon, J. E., Yoo, K. C., Macdonald, A. M., Yoon, H. I., Park, K. T., Yang, E. J., Kim, H. C., Lee, J. I., Lee, M. K., Jung, J., Park, J., Lee, J., Kim, S., Kim, S. S., Kim, K., and Kim, I.: Reviews and syntheses: Ocean iron fertilization experiments - past, present, and future looking to a future Korean Iron Fertilization Experiment in the Southern Ocean (KIFES) project, Biogeosciences, 15, 5847-5889, https://doi.org/10.5194/bg-15-5847-2018, 2018.

Yu, G., Zhang, Y., Yang, F., He, B., Zhang, C., Zou, Z., Yang, X., Li, N., and Chen, J.: Dynamic Ni/V Ratio in the Ship-Emitted Particles Driven by Multiphase Fuel Oil Regulations in Coastal China, Environ. Sci. Technol., 55, 15031-15039, https://doi.org/10.1021/acs.est.1c02612, 2021.

Yu, J. Z., Huang, X. F., Xu, J. H., and Hu, M.: When aerosol sulfate goes up, so does oxalate: Implication for the formation mechanisms of oxalate, Environ. Sci. Technol., 39, 128-133, https://doi.org/10.1021/es049559f, 2005.

Yu, J., Yao, X., and Zhou, Y.: Characteristics of aerosol aminiums over a coastal city in North China: Insights from the divergent impacts of marine and terrestrial influences. Sci. Total Environ., 918, 170672. https://doi.org/10.1016/j.scitotenv.2024.170672, 2024.

Yuan, C. -S., Hung, C. -M., Hung, K. -N., Yang, Z. -M., Cheng, P. -H., and Soong, K. -Y.: Route-based chemical significance and source origin of marine PM2.5 at three remote islands in East Asia: Spatiotemporal variation and long-range transport. Atmos. Pollut. Res., 14, 101762. https://doi.org/10.1016/j.apr.2023.101762, 2023.

Zhang, D., Iwasaka, Y., Shi, G., Zhang, J., Matsuki, A., and Trochkine, D.: Mixture state and size of Asian dust particles collected at southwestern Japan in spring 2000, J. Geophys. Res.-Atmos., 108(D24), 4760, https://doi.org/10.1029/2003JD003869, 2003.

Zhang, D., Iwasaka, Y., Matsuki, A., Ueno, K., and Matsuzaki, T.: Coarse and accumulation mode particles associated with Asian dust in southwestern Japan, Atmos. Environ., 40, 1205–1215, https://doi.org/10.1016/j.atmosenv.2005.10.037, 2006.

Zhang, G., Lin, Q., Peng, L., Yang, Y., Jiang, F., Liu, F., Song, W., Chen, D., Cai, Z., Bi, X., Miller, M., Tang, M., Huang, W., Wang, X., Peng, P. a., and Sheng, G.: Oxalate Formation Enhanced by Fe-Containing Particles and Environmental Implications, Environ. Sci. Technol., 53, 1269-1277, https://doi.org/10.1021/acs.est.8b05280, 2019.

Zhang, H., Li, R., Dong, S., Wang, F., Zhu, Y., Meng, H., Huang, C., Ren, Y., Wang, X., Hu, X., Li, T., Peng, C., Zhang, G., Xue, L., Wang, X., and Tang, M.: Abundance and Fractional Solubility of Aerosol Iron During Winter at a Coastal City in Northern China: Similarities and Contrasts Between Fine and Coarse Particles, J. Geophys. Res.-Atmos., 127, https://doi.org/10.1029/2021JD036070, 2022.

Zhang, J., Zhou, X., Wang, Z., Yang, L., Wang, J., and Wang, W.: Trace elements in PM2.5 in Shandong Province: Source identification and health risk assessment, Sci. Total. Environ., 621, 558-577, https://doi.org/10.1016/j.scitotenv.2017.11.292, 2018.

Zhang, L., Gao, Y., Wu, S., Zhang, S., Smith, K. R., Yao, X., and Gao, H.: Global impact of atmospheric arsenic on health risk: 2005 to 2015, P. Natl. Acad. Sci. USA, 117, 13975-13982, https://doi.org/10.1073/pnas.2002580117, 2020.

Zhang, Q., Jimenez, J. L., Canagaratna, M. R., Ulbrich, I. M., Ng, N. L., Worsnop, D. R., and Sun, Y.: Understanding atmospheric organic aerosols via factor analysis of aerosol mass spectrometry: a review, Anal. Bioanal. Chem., 401, 3045-3067, https://doi.org/10.1007/s00216-011-5355-y, 2011.

Zhang, T. L., Liu, J. Y., Xiang, Y. X., Liu, X. M., Zhang, J., Zhang, L., Ying, Q., Wang, Y. T., Wang, Y. N., Chen, S. L., Chai, F., and Zheng, M.: Quantifying anthropogenic emission of iron in marine aerosol in the Northwest Pacific with shipborne online measurements. Sci. Total Environ., 912, Article 169158, https://doi.org/10.1016/j.scitotenv.2023.169158, 2024.

Zhang, W., Peng, X., Bi, X., Cheng, Y., Liang, D., Wu, J., Tian, Y., Zhang, Y., and Feng, Y.: Source apportionment of PM2.5 using online and offline measurements of chemical components in Tianjin, China. Atmos. Environ., 244, 117942, https://doi.org/10.1016/j.atmosenv.2020.117942, 2021.

Zhang, Y., Cai, J., Wang, S., He, K., and Zheng, M.: Review of receptor-based source apportionment research of fine particulate matter and its challenges in China, Sci. Total. Environ., 586, 917-929, https://doi.org/10.1016/j.scitotenv.2017.02.071, 2017.

Zhang, Y., Deng, F., Man, H., Fu, M., Lv, Z., Xiao, Q., Jin, X., Liu, S., He, K., and Liu, H.: Compliance and port air quality features with respect to ship fuel switching regulation: a field observation campaign, SEISO-Bohai, Atmos. Chem. Phys., 19, 4899-4916, https://doi.org/10.5194/acp-19-4899-2019, 2019.

Zhang, Y., Schauer, J. J., Zhang, Y., Zeng, L., Wei, Y., Liu, Y., and Shao, M.: Characteristics of particulate carbon emissions from real-world Chinese coal combustion, Environ. Sci. Technol., 42, 5068-5073, https://doi.org/10.1021/es7022576, 2008.

Zhao, M., Zhang, Y., Ma, W., Fu, Q., Yang, X., Li, C., Zhou, B., Yu, Q., and Chen, L.: Characteristics and ship traffic source identification of air pollutants in China's largest port, Atmos. Environ., 64, 277-286, https://doi.org/10.1016/j.atmosenv.2012.10.007, 2013.

Zhao, R., Han, B., Lu, B., Zhang, N., Zhu, L., and Bai, Z.: Element composition and source apportionment of atmospheric aerosols over the China Sea. Atmos. Pollut. Res., 6, 191-201, http://doi.org/10.5094/APR.2015.023, 2015.

Zhou, S., Salter, M., Bertram, T., Azevedo, E. B., Reis, F., and Wang J.: Shoreline wave breaking strongly enhances the coastal sea spray aerosol population: Climate and airquality implications, Sci. Adv. 11, eadw0343, https://doi.org/10.1126/sciadv.adw0343, 2025.

Zhou, Y., Huang, X. H., Bian, Q., Griffith, S. M., Louie, P. K. K., and Yu, J. Z.: Sources and atmospheric processes impacting oxalate at a suburban coastal site in Hong Kong: Insights inferred from 1year hourly measurements, J. Geophys. Res.-Atmos., 120, 9772-9788, https://doi.org/10.1002/2015JD023531, 2015.

Zhou, Y.: Elevated Anthropogenic Contributions to Trace Elements in Marine Aerosols Compared to Coastal Qingdao in Eastern China. Figshiare [Dataset]. https://doi.org/10.6084/m9.figshare.29625746, 2026.

Zhu, W., Qi, Y., Tao, H., Zhang, H., Li, W., Qu, W., Shi, J., Liu, Y., Sheng, L., Wang, W., Wu, G., Zhao, Y., Zhang, Y., Yao, X., Wang, X., Yi, L., Ma, Y., and Zhou, Y.: Investigation of a haze-to-dust and dust swing process at a coastal city in northern China part I: Chemical composition and contributions of anthropogenic and natural sources, Sci. Total. Environ., 851, 158270, https://doi.org/10.1016/j.scitotenv.2022.158270, 2022a.

Zhu, Y., Li, W., Wang, Y., Zhang, J., Liu, L., Xu, L., Xu, J., Shi, J., Shao, L., Fu, P., Zhang, D., and Shi, Z.: Sources and processes of iron aerosols in a megacity in Eastern China, Atmos. Chem. Phys., 22, 2191-2202. https://doi.org/10.5194/acp-22-2191-2022, 2022b.

Zhuang, G., Yi, Z., Duce, R. A., and Brown, P. R.: Link between iron and sulphur cycles suggested by detection of Fe(n) in remote marine aerosols. Nature, 355, 537-539. https://doi.org/10.1038/355537a0, 1992

Supplement of

Elevated Anthropogenic Contributions to Trace Elements in Marine Aerosols Compared to Coastal Qingdao in Eastern China

Yuxuan Qi et al.

Corresponding to: Yang Zhou (yangzhou@ouc.edu.cn)

Contents of this file

Supplemental Texts

Text S1: Quality assurance and quality control

(a) Trace elements

Assessment and implications of procedural blanks: Blank filters were processed and analyzed following the identical protocol to that of the samples. Average blank concentrations and standard deviations for all trace elements are summarized in Table S1. The impact of blanks was evaluated by quantifying their typical percentage fraction to the measured sample concentrations. For most elements, the blank fractions were below 10%. Among these, seven elements exhibited particularly low blank levels (<5%), with Fe blanks notably evaluated at 3.1% (marine samples) and 4.0% (Qingdao samples). Although the blank fractions for Al were higher in marine samples, it is crucial to note that all reported data have undergone rigorously blank-correction. Furthermore, Al was not included as an input species in our PMF source apportionment. With these measures, uncertainties due to filter blanks have been minimized and are not expected to influence the results considerably.

Digestion procedure and environmental control: The acid digestion of aerosol samples, including the evaporation to dryness step, was conducted inside a standard fume hood under ambient laboratory conditions. The following stringent measures were implemented to assess and mitigate potential contamination, especially critical for the low metal concentrations in cases of marine aerosols: (i) All sample processing steps were performed in parallel with procedural blank filters. (ii) All labware underwent rigorous acid cleaning: rinsed six times with Milli-Q water ($\geqslant$18.0 MΩ·cm), immersed in 20% HNO_3 bath for 24-hour, another six-time rinse with Milli-Q water, and finally dried in a clean bench. Filter samples were cut using a pre-cleaned ceramic knife and ceramic tweezers. (iii) All analytical results were blank-corrected using the procedural blanks. As evidenced by low blank levels for most elements, contamination introduced during the experimental process was effectively controlled and did not compromise data quality or the integrity of the scientific conclusions

(b) Water-soluble ions

Standard solutions were analyzed after every 10 samples to monitor instrumental precision and accuracy. Blank filters were analyzed at the same frequency to quantify and subtract any contamination introduced during the sample extraction process.

(c) Analysis of OC and EC

The concentrations of OC and EC were measured using a Sunset OC/EC analyzer (RT-3131, Sunset Laboratory, OR, USA). A 2.0 cm^2 punch of each quartz filter sample was analyzed following the National Institute for Occupational Safety and Health (NIOSH) 5040 thermal-optical transmittance (TOT) protocol.

The analysis involved a two-stage heating process. Initially, the punch sample was heated in a pure helium (He) atmosphere through a series of temperature steps to volatilize and quantify OC. During this stage, a portion of OC was pyrolyzed, forming pyrolyzed carbon (PC). Subsequently, the atmosphere was switched to a mixture of He and oxygen (He/O_2). In this oxidative environment, the sample was further heated, causing the remaining EC and the previously formed PC to combust. A critical correction for the PC formed during the He phase was applied. This was achieved by continuously monitoring the transmittance of a laser through the filter (Wu et al., 2016). The laser transmittance decreased as PC formed and recovered as PC and EC were combusted in the He/O_2 phase. The point at which the laser transmittance returns to its initial value is defined as the OC/EC split point. The carbon detected before this split point is defined as OC, and the carbon detected after is defined as EC. The carbonaceous gases produced in both stages were converted to carbon dioxide (CO_2) in a manganese dioxide (MnO_2) oxidation oven and then quantified by a flame ionization detector (FID) or a non-dispersive infrared (NDIR) detector.

The method detection limit is approximately 0.2 μgC m^{-3} for filter analysis, with an analytical uncertainty (standard deviation) between 4% and 6%. Obtained data were calibrated using a standard curve, and routine quality assurance includes the analysis of calibration standards and blank filters.

Text S2: Detailed description of PMF analysis

PMF solution evaluation: Multiple factors ranging from 6 to 10 were thoroughly evaluated to determine the optimal solution. The stability and reliability of the factor solutions were assessed using the displacement (DISP) and bootstrap (BS) uncertainty estimation methods (Norris et al., 2014). Ultimately, an 8-factor solution emerged as the most robust and interpretable. In contrast, the 7-factor solution failed to distinguish the industrial emissions from dust (Fig.S1a). The 9-factor solution tended to resolve an additional factor; however, it exhibited relatively low BS mapping values (58%, 67%, and 73%) for several factors (Fig.S1b and Table S2). The 8-factor solution demonstrated the highest stability. The mapping percentages using the BS uncertainty method exceeded 80% for all factors (Table S3), surpassing the performances of the 7-factor and 9-factor solutions (Tables S4 and S2). Moreover, the DISP analysis showed no occurrences of factor swapping and no reduction in the model fit statistic Q (both %dQ and the error code were 0), further validating the stability and interpretation of the 8-factor solution.

Based on the established 8-factor PMF solution, a detailed evaluation of its performance in simulating Fe concentrations was conducted. The results showed that while the model performed well for most elements (e.g.,

Fig.S11b and c), the PMF-resolved total Fe in marine aerosols in summer (191.5 ng m^{-3}) was substantially higher than the measured concentration (109.8 ng m^{-3}), indicating an overestimation in the absolute source concentrations for Fe in this specific scenario. Therefore, the reported concentrations by PMF for marine Fe in summer should be interpreted as upper-bound estimates. Crucially, the strong linear correlation ($r^2 = 0.98$, $p < 0.01$) between the PMF-simulated and measured Fe concentrations ($r^2 = 0.76$, $p = 0.02$ for summer marine samples; Fig.S11a) indicated that the overestimation was proportional. This high coherence in temporal trends strongly suggested that the relative source contributions for Fe remained robust.

Text S3: Enrichment factor (EF) calculation

The EF was calculated to assess the anthropogenic influence on trace elements using Al as a reference element (R). The calculation followed the equation:

$$EF = \frac{(C_X/C_R)_{aerosol}}{(C\prime_X/C\prime_R)_{crustal}} \quad (1)$$

Where C_X is the concentration of element X in aerosols, C_R is the concentration of the reference element R in aerosols, and the denominator is the ratio of the content of element X to R in the Earth's crust. The crust values were taken from the upper continental crust composition reported by Taylor (1964).

Supplemental Figures

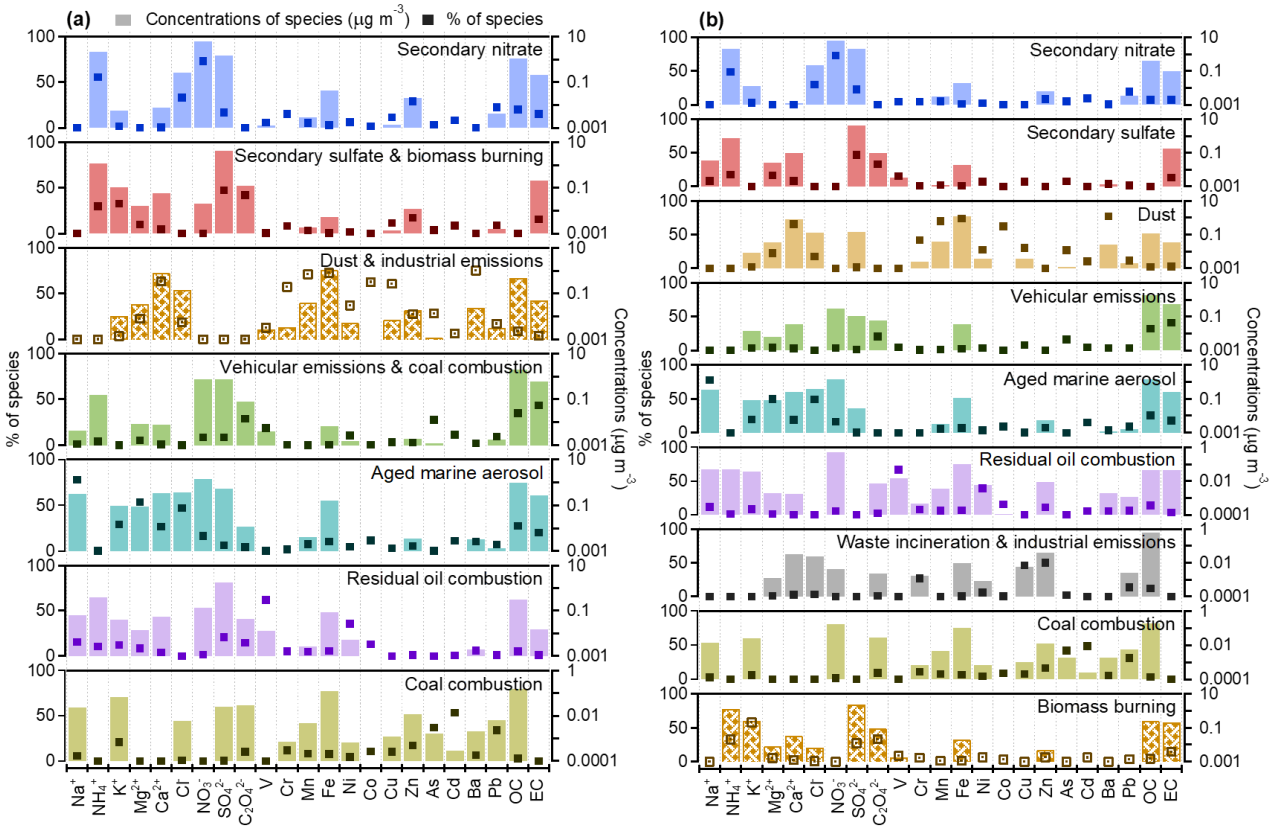

Figure S1: PMF resolved factor profiles (dark points represent the percentages and light rectangles represent the concentrations of each species in each factor) of (a) 7-factor and (b) 9-factor solution.

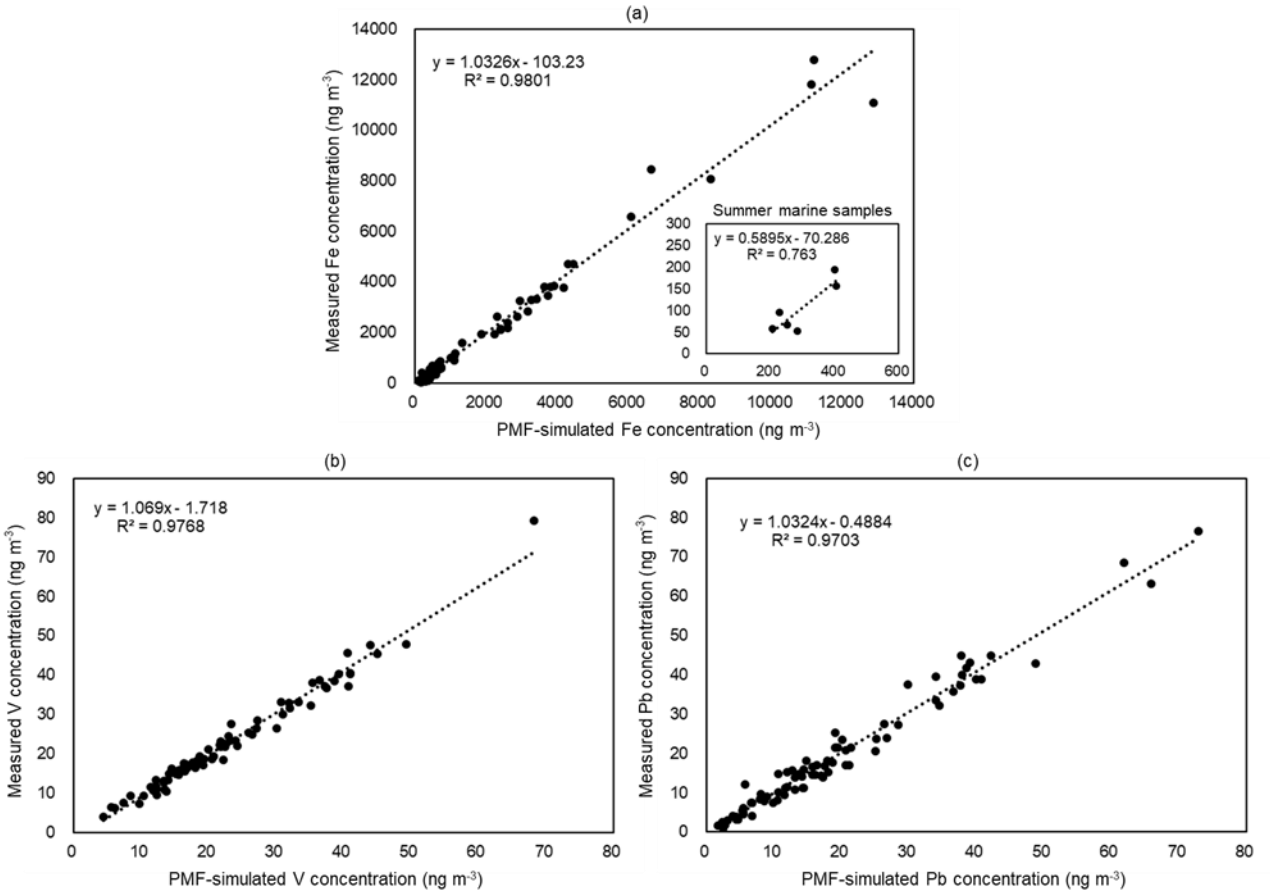

Figure S2. Comparison of measured and PMF-simulated concentrations (ng m^{-3}): (a) Fe, (b) V, and (c) Pb.

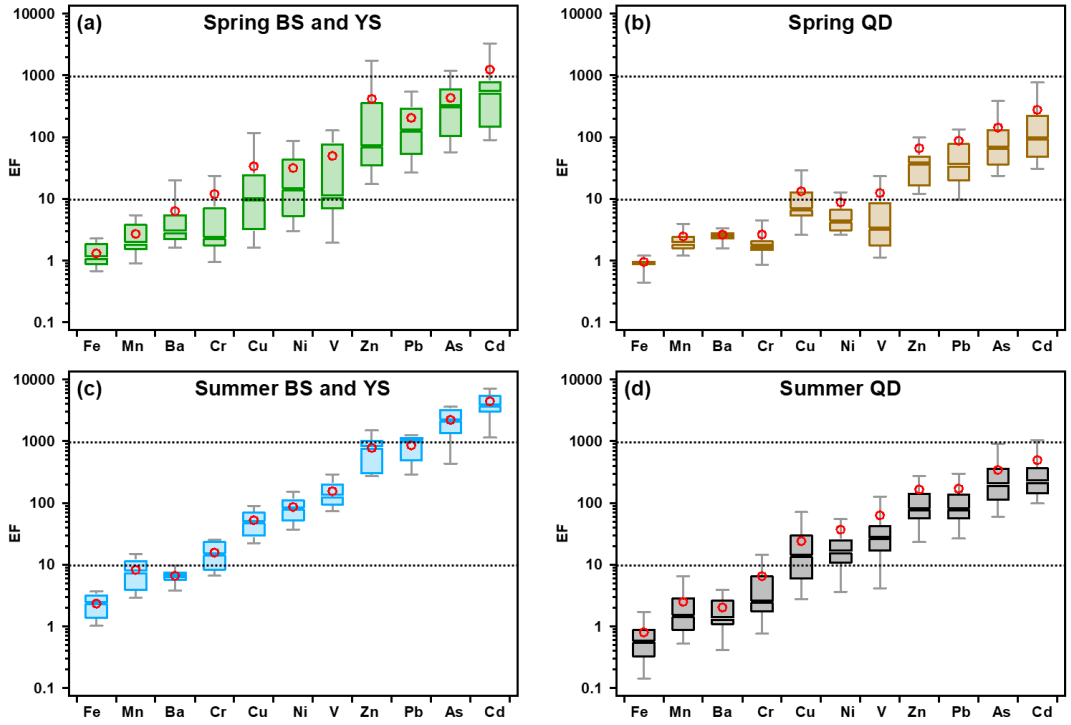

Figure S3: Elemental EFs in fine particles over (a) spring BS and YS, (b) spring Qingdao (QD), (c) summer BS and YS, and (d) summer QD. 25th and 75th percentile boxes; 10th and 90th percentile whiskers; the solid line is the median value, and the red circle is the mean value. (It can be seen that the EFs over the BS and YS are generally higher than those in QD.)

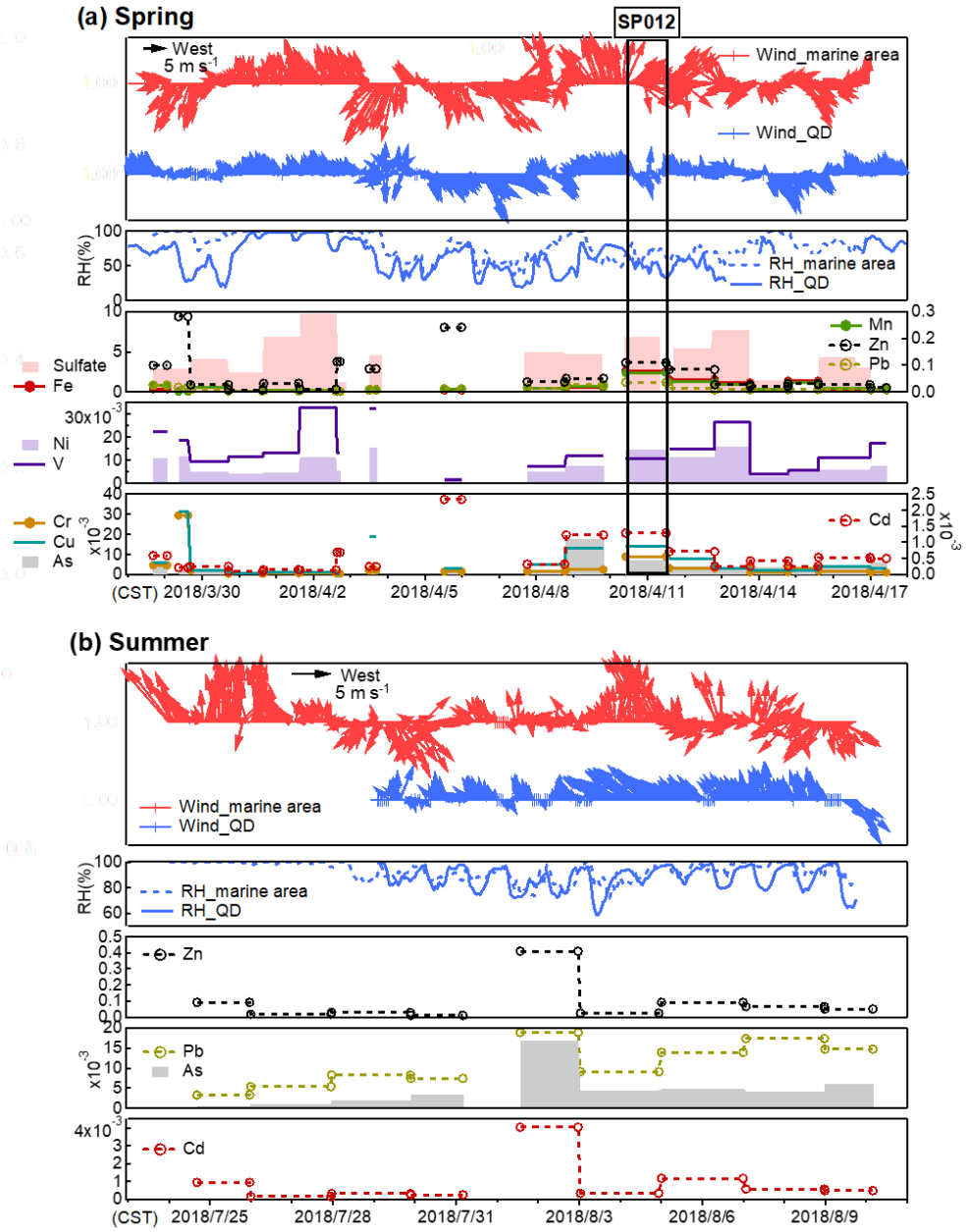

Figure S4. Temporal variations of meteorological parameters and selected species concentrations (μg m^{-3}) in (a) spring and (b) summer. "SP012" marked in (a) show the information about the sampling period for sample SP012. "Marine area" refers to the BS and YS.

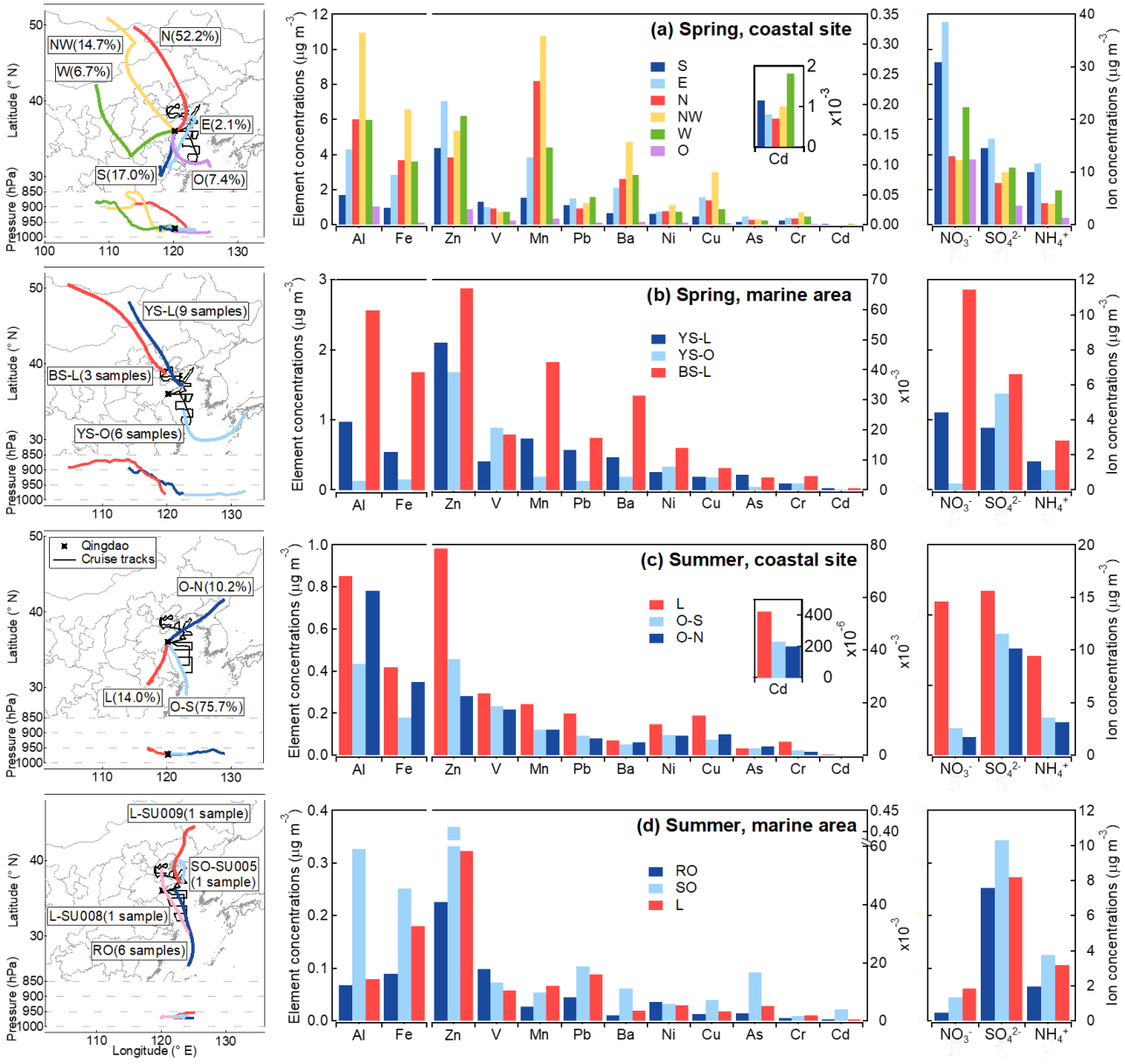

Figure S5. To explore the influence of air mass history on variations in trace element abundances, the backward trajectories calculated by HYSPLIT model were classified into six categories in spring and three in summer at the coastal city site (Qingdao), using a systematic clustering method implemented in the software SPSS (Statistical Product and Service Solutions) Statistics v21. For the cruise missions, the trajectory endpoints corresponded to the cruise coordinates, thus the samples were manually classified into three categories in both seasons. Averaged 72 h backward trajectories of air masses arriving at 300 m altitudes and the averaged concentrations of trace elements and ions of individual clusters in spring at (a) the coastal site (Qingdao) and (b) marine areas (BS and YS) and in summer at (c) the coastal site and (d) marine areas. The black star indicates the coastal site, Qingdao. The solid black line indicates the cruise tracks. "YS-O" means "YS-ocean". Al and Fe use the left labels; other elements use

the right labels.

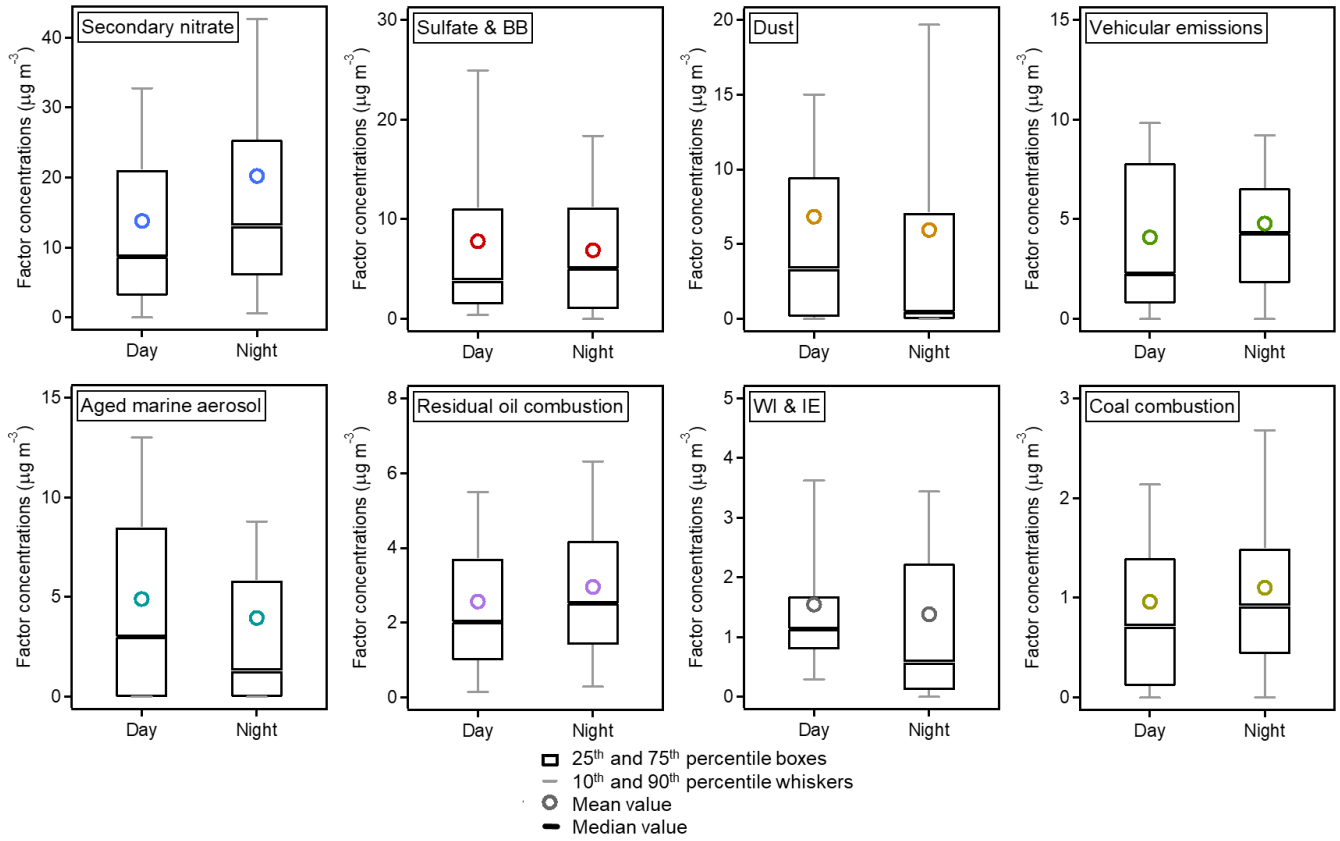

Figure S6. Diurnal variations of individual factor contributions from PMF results in Qingdao. (29 daytime and 26 nighttime samples were collected, respectively. 25th and 75th percentile boxes, 10th and 90th percentile whiskers; the solid black line is the median value, and the circle is the mean value.) Sulfate & BB represents sulfate & biomass burning. WI & IE represents waste incineration & industrial emissions.

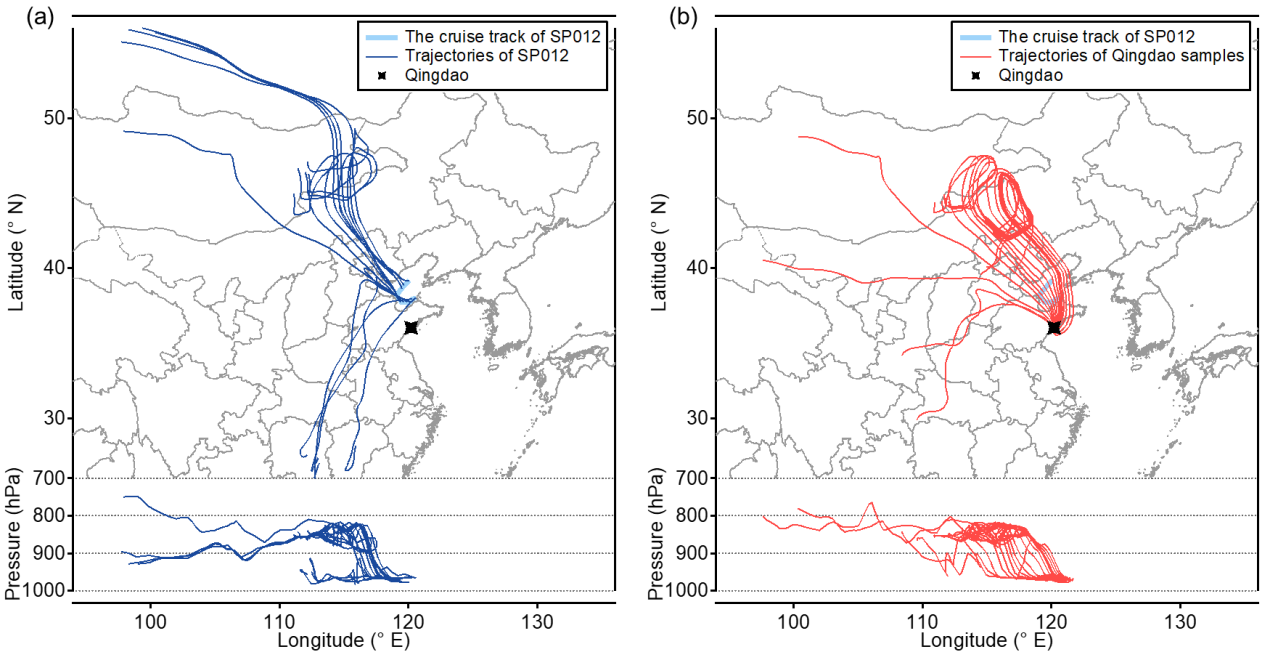

Figure S7. 72 h backward trajectories of air masses arriving 300 m altitude of (a) the marine sample SP012 and (b) its corresponding Qingdao samples.

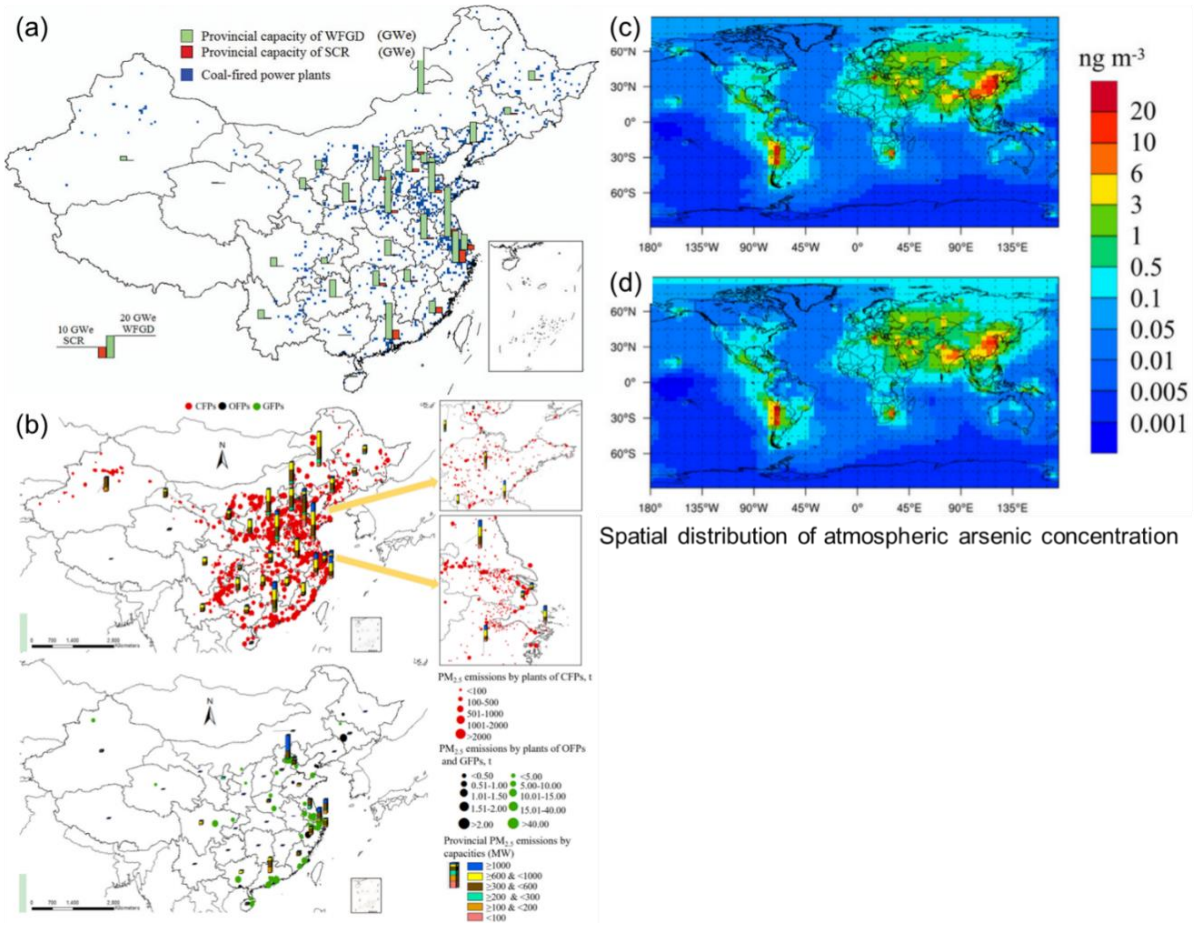

Figure S8. (a) Geographical distribution of coal-fired power plants in China, 2010 (Tian et al., 2014). WFGD represents wet flue gas desulfurization. SCR represents selective catalytic reduction. (b) Spatial distribution of $PM_{2.5}$ emissions by coal-fired power plants in China, 2014 (Wang et al., 2016). CFPs, OFPs, and GFPs represent coal-fired power plants, oil-fired power plants, and natural gas-fired power plants, respectively. Spatial distribution of atmospheric arsenic (As) concentration from GEO-Chem in (c) 2005 and (d) 2015 (Zhang et al., 2020).

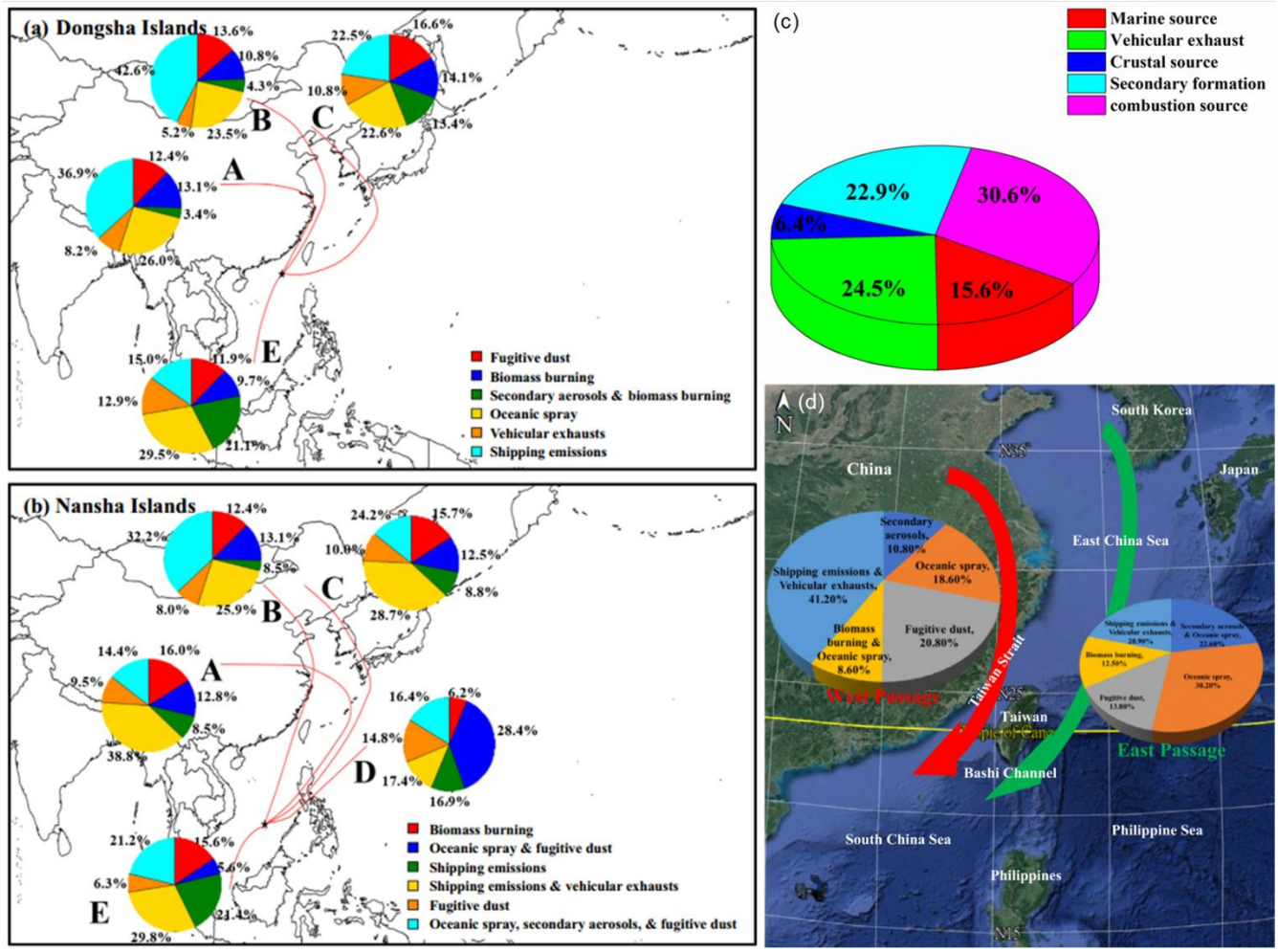

Figure S9. (a) Source contribution resolved from the PMF analysis of $PM_{2.5}$ at (a) the Dongsha Islands and (b) the Nansha Islands for the transport route-based cluster analysis (A: Central China; B: North China; C: Korea, Japan, and Northeast China; D: the Philippines and the West Pacific Ocean; E: the South China Sea) (Yen et al., 2022b). (c) The contribution of different sources in $PM_{2.5}$ in the Eastern China Sea (Sun et al., 2022). (d) Source apportionment of marine fine particles at two islands through the west and east passages of the Taiwan Island (Yen et al., 2022a).

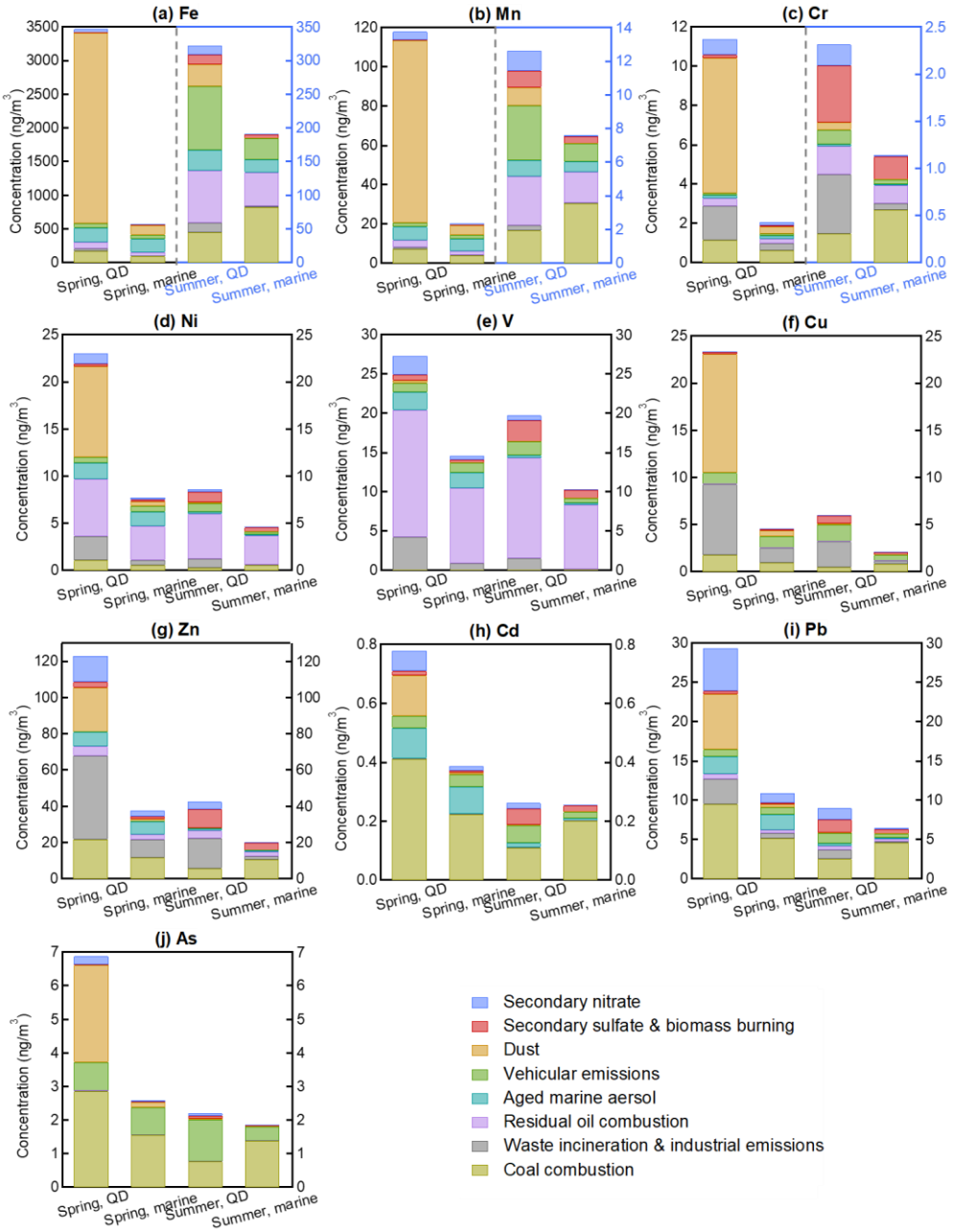

Figure S10. Concentrations of various source factors to individual elements based on PMF results. "marine" refers to the BS and YS. For Fe, Mn, and Cr, the left and right axes (spring vs. summer) use different scales, distinguished by color (right axis in blue).

Supplemental Tables

Table S1. Average blank concentrations (μg L^{-1}), standard deviation (μg L^{-1}), and typical blank fractions (%) for trace elements in ICP-MS analytical solution.

Element	Average blank (μg L^{-1})	Standard deviation (μg L^{-1})	Typical blank fraction (%)*	
			Marine	Qingdao
Al	52.7	3.1	43.4	11.8
Fe	6.0	8.0	3.1	4.0
Mn	0.1	0.1	3.8	1.1
Ba	0.1	0.1	3.8	4.6
Zn	2.3	2.6	17.2	10.1
V	0.6	0.3	11.2	9.7
Pb	0.0	0.1	0.7	0.6
Ni	0.2	0.3	-	9.4
Cu	0.3	0.3	4.3	12.8
As	0.0	0.0	0.4	-
Cr	0.0	0.0	4.6	4.6
Cd	0.0	0.0	16.0	9.7
Co	0.0	0.0	4.5	5.3

*. Typical blank fractions were estimated as (average blank concentration / typical sample concentration) × 100%. Typical sample concentrations were derived from the median values from marine and Qingdao samples, respectively. A dash (-) indicates concentrations below the detection limit for marine or Qingdao samples.

Table S2. Bootstrap (BS) mapping of 9-factor solution based on PMF.

	Base factor 1	Base factor 2	Base factor 3	Base factor 4	Base factor 5	Base factor 6	Base factor 7	Base factor 8	Base factor 9	Unmapped
Boot factor 1	97	0	0	0	0	1	0	2	0	0
Boot factor 2	0	99	0	0	1	0	0	0	0	0
Boot factor 3	0	0	100	0	0	0	0	0	0	0
Boot factor 4	0	1	2	93	1	1	0	1	1	0
Boot factor 5	4	1	7	1	58*	2	5	10	9	3
Boot factor 6	1	2	12	3	0	67*	0	0	12	3
Boot factor 7	0	0	1	1	0	0	98	0	0	0
Boot factor 8	1	1	5	2	5	2	1	73*	10	0
Boot factor 9	0	0	0	0	0	0	0	0	100	0

*. The mapping percentages were less than 80% using the BS uncertainty method.

Table S3. BS mapping of 8-factor solution based on PMF.

	Base factor 1	Base factor 2	Base factor 3	Base factor 4	Base factor 5	Base factor 6	Base factor 7	Base factor 8	Unmapped
Boot factor 1	100	0	0	0	0	0	0	0	0
Boot factor 2	6	81	0	4	2	0	2	2	3
Boot factor 3	1	1	95	0	1	0	0	2	0
Boot factor 4	0	0	0	100	0	0	0	0	0
Boot factor 5	3	1	1	1	92	1	0	1	0
Boot factor 6	0	0	0	0	0	100	0	0	0
Boot factor 7	0	0	0	0	0	0	100	0	0
Boot factor 8	0	0	0	0	0	0	0	100	0

Table S4. BS mapping of 7-factor solution based on PMF.

	Base factor 1	Base factor 2	Base factor 3	Base factor 4	Base factor 5	Base factor 6	Base factor 7	Unmapped
Boot factor 1	80	5	3	1	1	3	2	5
Boot factor 2	0	100	0	0	0	0	0	0
Boot factor 3	5	6	79*	6	1	1	0	2
Boot factor 4	0	1	0	99	0	0	0	0
Boot factor 5	0	0	0	0	100	0	0	0
Boot factor 6	0	1	0	2	0	97	0	0
Boot factor 7	0	0	0	0	0	1	99	0

*. The mapping percentages were less than 80% using the BS uncertainty method.

Table S5. Comparison of concentrations (ng m^{-3}) of trace elements over the BS and YS in this study with other studies on $PM_{2.5}$ in oceanic regions of China.

Area	Time	Al	Fe	Zn	V	Mn	Pb	Ba	Ni	Cu	As	Cr	Cd	Reference
BS and YS	2018.3–4	1043.2	648.6	49.9	14.2	18.4	11.8	13.0	8.0	5.0	3.7	2.6	0.5	This study
	2018.7–8	71.1	109.8	44.9	16.2	6.5	9.9	2.3	6.4	2.6	3.2	1.4	0.5	
BS	2018.3–4	2562.8	1682.2	67.2	18.5	42.6	17.5	31.5	14.0	7.4	4.1	4.6	0.7	
	2018.7–8	72.6	162.3	79.7	13.1	9.6	15.5	2.9	5.8	3.0	4.6	1.9	0.9	
YS	2018.3–4	689.2	407.9	45.8	13.2	12.8	10.5	8.7	6.6	4.4	3.7	2.1	0.5	
	2018.7–8	70.5	92.7	33.6	17.3	5.5	8.0	2.1	6.5	2.4	2.8	1.2	0.4	
YS	2011.3–4	2803.3	1111.8	74.2	20.7	14.8	18.9	-	20.1	11.5	8.6	-	-	Zhao et al., 2015
ECS	2018.4–5	244.1	223.0	37.9	22.4	10.5	10.6	8.5	8.9	8.0	3.8	14.7	0.3	Sun et al., 2022
Pengjiayu, ECS*	2019.9–2020.8	109.9	71.7	5.7	0.6	1.9	1.5	-	0.4	-	-	-	0.1	Hsieh et al., 2023
Huaniao Island, ECS**	2015–2018	-	160.0	-	-	-	-	-	-	-	-	-	-	Yang et al., 2020
Penghu Islands (PH)	2017.8–9	150	180	40	20	30	40	-	10	20	-	20	<5	Yuan et al., 2023
Dongsha Islands (DS)		80	70	50	<5	10	20	-	<5	20	-	10	<5	
Nansha Islands (NS)***		50	50	30	<5	<5	<5	-	<5	20	-	10	<5	
PH	2018.3–4	450	370	150	80	40	100	-	70	30	-	50	30	
DS		360	310	120	60	30	80	-	60	30	-	40	30	
NS		60	70	40	10	10	50	-	20	10	-	20	20	

*. The data in this study were derived from paticles with aerodynamic diameters less than 3.1 μm ($PM_{3.1}$).
**. The data in this study were derived from paticles with aerodynamic diameters less than 1.8 μm ($PM_{1.8}$).
***. The three remote islands (PH, DS, and NS) were located from the south Taiwan Strait (TS) to the north South China Sea (SCS).

Table S6. Comparison of concentrations (ng m^{-3}) of trace elements in Qingdao in this study with other studies on $PM_{2.5}$ in typical cities of China.

City	Type	Time	Al	Fe	Zn	V	Mn	Pb	Ba	Ni	Cu	As	Cr	Cd	Reference
Qingdao	Coastal	2018.3–4	5573.5	3347.3	120.1	26.4	127.8	29.3	70.3	21.9	39.5	7.6	11.1	0.8	This study
		2018.7–8	572.9	228.3	40.9	19.2	11.1	8.6	4.4	8.3	7.4	2.7	2.4	0.3	
Qingdao	Coastal	2018.6–7	548.9	347.3	91.7	9.4	~11	22.5	~11	-	-	-	-	-	Li et al., 2018
Qingdao*	Coastal	2019.11–12	935.5	801.0	57.1	2.3	29.9	14.9	19.2	2.5	43.5	2.5	4.3	0.5	Zhang et al., 2021
Beijing	Inland	2005.3–2006.2	790	1130	530	30	90	240	210	20	70	20	50	50	Chen et al., 2008
Tianjin	Coastal	2017.10–2018.8	-	409	136	2	20	31	-	12	33	18	-	-	Zhang et al., 2021
Shanghai	Coastal	2016.3–2017.2	-	410	120	13	32	27	24	6	12	6.6	4.5	9.6	Chang et al., 2018
Shanghai**	Coastal	2004.4–2005.4	-	950	349	9	51	143	12	8	29	28	15	3.7	Chen et al., 2008
Ningbo	Coastal	2014.3–5	1430	1420	229	9.4	-	68.9	-	10.0	20.1	-	14.1	-	Ming et al., 2017
		2014.6–8	676	354	65.3	3.2	-	14.7	-	4.0	4.6	-	9.3	-	
Xiamen	Coastal	2017.1–2018.1	210	290	86.7	10.6	14.3	19.3	11.3	7.1	7.2	1.6	8.5	0.5	Wu et al., 2020
Guangzhou	Coastal	2008.12–2009.2	-	1850	1360	20	150	450	70	-	190	40	70	20	Yang et al., 2011
Hangzhou***	Near-coastal	2018.11–2020.1	2194.4	2529.1	160.4	2.8	33.2	36.0	59.9	22.1	46.1	-	21.2	-	Zhu et al., 2022

*. The data in this study were derived from paticles with aerodynamic diameters less than 1 μm (PM_1).

**. An urban-residential site, Putuo.

***. The data were obtained from the analysis using an energy dispersive X-ray fluorescence (EDXRF) spectrometer (in μg cm^{-2}) and have been converted by the authors of this study (in ng m^{-3}).

Table S7. Pearson correlations (r) of PMF factor contributions with meteorological parameters (relative humidity (RH) and wind speed (WS)), and gas pollutants concentrations (SO_2, NO_2, O_3 and CO).

Factor	RH	WS	SO_2	NO_2	O_3	CO
Secondary nitrate	–0.18	–0.17	0.30*	0.45**	0.26*	0.39**
Secondary sulfate & biomass burning	0.36**	–0.25*	-0.46**	-0.52**	0.39**	0.54**
Dust	–0.72**	0.18	0.19	0.35**	–0.13	–0.13
Dust (spring, coastal)	-	0.43*	-	-	-	-
Vehicular emissions	0.01	–0.36**	0.11	0.10	–0.37**	0.30*
Vehicular emissions (summer)	-	-	-	0.78**	-	-
Aged marine aerosol	–0.63**	0.35**	0.31*	0.46**	–0.05	–0.03
Residual oil combustion	0.06	–0.24*	0.38**	0.19	–0.06	–0.05
Waste incineration & industrial emissions	–0.33**	0.10	0.31*	0.50**	–0.06	0.24
Coal combustion	–0.23*	0.00	0.35**	0.54**	0.18	0.27*

Note. The highest correlation coefficients for each factor are denoted in bold. No gas pollutants data was available for the cruise campaign. The meteorological parameters of the former eight samples in summer Qingdao are missing values.

*. Correlation is significant at the 0.05 level (2-tailed).

**. Correlation is significant at the 0.01 level (2-tailed).

Table S8. The information of averaged 72 h air mass backward trajectory clusters arriving at the coastal site (Qingdao) and marine area (BS and YS) in spring and summer.

Campaign	Cluster	Detailed information	Frequency
Spring, coastal site	N (North)	From the north and passed the Inner Mongolia Autonomous region and Liaoning Province	52.2%
	NW (Northwest)	From the northwest and passed the Inner Mongolia Autonomous and BTH region	14.7%
	W (West)	From the Inner Mongolia Autonomous region and passed Shaanxi and Henan Provinces	6.7%
	S (South)	From East China near the Yangtze River Delta (YRD)	17.0%
	E (East)	From East China near YRD and passed YS before reversing to the Shandong Peninsula	2.1%
	O (Ocean)	Mainly from ECS and passed YS	7.4%
Spring, marine area	BS-L (BS-Land)	BS samples influenced by the continent air masses	Three samples
	YS-L (YS-Land)	YS samples influenced by the continent air masses	Nine samples
	YS-O (YS-Ocean)	YS samples influenced by the marine air masses	Six samples
Summer, coastal site	L (Land)	Passed the continent of East China before arriving at QD	14.0%
	O-S (Ocean-South)	From ECS in the south	75.7%
	O-N (Ocean-North)	From Korean Peninsula in the north	10.2%
Summer, marine area	L (Land)	Two samples influenced by the continent air masses, one passed the coastline of southeastern China (L-SU008), another from the northern China (L-SU009)	Two samples
	RO (Remote oceans)	Samples influenced by remote ocean air masses	Six samples
	SO (Surrounding oceans)	BS sample influenced by the air masses lingered over the CBS region	One sample, SU005

Table S9. Percentage contributions (%) of various source factors to individual elements based on PMF. "Marine" refers to the BS and YS areas, while "coastal" refers to Qingdao, hereinafter the same.

Element	Season	location	Secondary nitrate	Sulfate & BB	Dust	VE	Aged marine aerosol	ROC	WI & IE	CC
Fe	Spring	Coastal	1.4	0.1	81.6	1.8	6.1	2.8	1.1	4.9
		Marine	1.9	0.3	25.4	11.0	33.6	10.2	1.4	16.2
	Summer	Coastal	4.3	4.3	10.3	29.1	9.5	24.1	4.3	14.1
		Marine	0.6	2.9	-	16.7	9.8	26.1	0.8	43.2
Mn	Spring	Coastal	3.6	0.2	78.6	1.8	5.7	3.1	0.8	6.2
		Marine	4.5	0.7	23.4	10.6	29.7	10.7	0.9	19.5
	Summer	Coastal	9.3	7.9	8.6	25.7	7.6	22.9	2.6	15.4
		Marine	1.2	5.2	-	14.4	7.7	24.4	0.5	46.5
Cr	Spring	Coastal	7.1	1.5	60.4	0.9	1.5	3.3	15.3	10.1
		Marine	8.2	4.2	16.9	4.8	7.5	10.6	17.7	30.0
	Summer	Coastal	9.5	26.1	3.5	6.5	1.1	12.8	27.3	13.3
		Marine	1.5	21.1	-	4.4	1.3	16.6	5.9	49.1
Ni	Spring	Coastal	4.6	1.3	41.9	2.6	7.5	26.2	11.2	4.7
		Marine	2.9	2.1	6.4	7.7	20.2	46.2	7.1	7.5
	Summer	Coastal	3.4	12.7	1.3	10.3	2.9	55.2	10.8	3.3
		Marine	0.5	9.5	-	6.6	3.3	66.6	2.2	11.3
V	Spring	Coastal	8.7	2.7	1.1	4.4	8.2	59.4	15.5	-
		Marine	3.5	2.6	0.1	8.1	13.8	65.7	6.2	-
	Summer	Coastal	3.3	13.5	0.0	9.0	1.6	64.8	7.8	-
		Marine	0.5	10.3	-	5.9	1.9	79.8	1.6	-
Cu	Spring	Coastal	-	1.0	54.0	5.2	-	-	32.2	7.6
		Marine	-	2.6	14.3	26.5	-	-	35.3	21.3
	Summer	Coastal	-	13.8	2.5	30.1	-	-	45.7	7.9
		Marine	-	15.7	-	29.2	-	-	13.9	41.2
Zn	Spring	Coastal	11.7	2.4	20.2	-	6.4	4.2	37.5	17.7
		Marine	8.2	4.0	3.4	-	18.8	8.1	26.0	31.5
	Summer	Coastal	9.3	24.7	0.7	-	2.6	9.6	39.4	13.7
		Marine	1.6	20.7	-	-	3.4	12.9	8.8	52.5
Cd	Spring	Coastal	8.8	1.9	17.6	5.2	13.2	0.3	-	53.0
		Marine	3.8	2.0	1.8	10.3	23.9	0.3	-	57.8
	Summer	Coastal	7.2	20.9	0.6	22.9	5.6	0.7	-	42.1
		Marine	0.6	8.6	-	8.0	3.6	0.4	-	78.8
Pb	Spring	Coastal	18.4	1.5	23.9	3.1	7.6	2.1	10.9	32.5
		Marine	10.6	2.1	3.3	8.3	18.5	3.4	6.2	47.6
	Summer	Coastal	16.5	17.5	0.9	15.0	3.6	5.4	12.8	28.3
		Marine	1.8	9.7	-	7.1	3.0	4.9	1.9	71.6
As	Spring	Coastal	3.5	0.3	41.9	12.3	-	-	0.5	41.5
		Marine	2.0	0.5	5.7	31.9	-	-	0.3	59.7
	Summer	Coastal	3.0	3.7	1.5	56.6	-	-	0.5	34.6
		Marine	0.3	1.8	-	22.8	-	-	0.1	75.0

Note. Sulfate & BB represents sulfate & biomass burning. VE represents vehicular emissions. ROC represents residual oil combustion. WI & IE represents waste incineration & industrial emissions. CC represents coal combustion. A dash (-) indicates that the species is entirely absent from the factor profile for that period, not that its concentration is rounded to zero, hereinafter the same.

Table S10. Concentrations (ng m^{-3}) of various source factors to individual elements based on PMF.

Element	Season	location	Secondary nitrate	Sulfate & BB	Dust	VE	Aged marine aerosol	ROC	WI & IE	CC
Fe	Spring	Coastal	50.12	3.80	2832.00	63.72	212.82	98.67	38.36	170.19
		Marine	10.72	1.99	145.19	62.62	191.58	58.26	8.14	92.36
	Summer	Coastal	13.73	13.76	33.33	94.03	30.60	77.79	13.92	45.46
		Marine	1.11	5.49	-	31.90	18.75	50.02	1.48	82.77
Mn	Spring	Coastal	4.29	0.28	92.73	2.20	6.70	3.67	0.89	7.30
		Marine	0.92	0.14	4.75	2.16	6.03	2.17	0.19	3.96
	Summer	Coastal	1.17	1.00	1.09	3.24	0.96	2.89	0.32	1.95
		Marine	0.09	0.40	-	1.10	0.59	1.86	0.03	3.55
Cr	Spring	Coastal	0.80	0.17	6.88	0.10	0.17	0.37	1.74	1.15
		Marine	0.17	0.09	0.35	0.10	0.16	0.22	0.37	0.63
	Summer	Coastal	0.22	0.60	0.08	0.15	0.02	0.30	0.63	0.31
		Marine	0.02	0.24	-	0.05	0.02	0.19	0.07	0.56
Ni	Spring	Coastal	1.06	0.30	9.63	0.60	1.73	6.04	2.58	1.07
		Marine	0.23	0.16	0.49	0.59	1.56	3.57	0.55	0.58
	Summer	Coastal	0.29	1.10	0.11	0.89	0.25	4.76	0.96	0.29
		Marine	0.02	0.44	-	0.30	0.15	3.06	0.10	0.52
V	Spring	Coastal	2.37	0.74	0.31	1.21	2.23	16.23	4.23	-
		Marine	0.51	0.38	0.02	1.18	2.01	9.58	0.90	-
	Summer	Coastal	0.65	2.66	0.00	1.78	0.32	12.80	1.54	-
		Marine	0.05	1.06	-	0.60	0.20	8.23	0.16	-
Cu	Spring	Coastal	-	0.23	12.59	1.22	-	-	7.51	1.77
		Marine	-	0.12	0.64	1.20	-	-	1.59	0.96
	Summer	Coastal	-	0.82	0.15	1.80	-	-	2.73	0.47
		Marine	-	0.33	-	0.61	-	-	0.29	0.86
Zn	Spring	Coastal	14.36	2.90	24.79	-	7.83	5.16	46.12	21.82
		Marine	3.07	1.52	1.27	-	7.05	3.05	9.79	11.84
	Summer	Coastal	3.93	10.50	0.29	-	1.13	4.07	16.74	5.83
		Marine	0.32	4.19	-	-	0.69	2.62	1.78	10.61
Cd	Spring	Coastal	0.07	0.02	0.17	0.04	0.10	0.00	-	0.41
		Marine	0.01	0.01	0.01	0.04	0.09	0.00	-	0.22
	Summer	Coastal	0.02	0.05	0.00	0.06	0.01	0.00	-	0.11
		Marine	0.00	0.02	-	0.02	0.01	0.00	-	0.20
Pb	Spring	Coastal	5.41	0.43	7.02	0.92	2.24	0.62	3.19	9.53
		Marine	1.16	0.23	0.36	0.90	2.01	0.37	0.68	5.17
	Summer	Coastal	1.48	1.57	0.08	1.35	0.32	0.49	1.16	2.55
		Marine	0.12	0.63	-	0.46	0.20	0.31	0.12	4.64
As	Spring	Coastal	0.24	0.02	2.88	0.84	-	-	0.03	2.86
		Marine	0.05	0.01	0.15	0.83	-	-	0.01	1.55
	Summer	Coastal	0.07	0.08	0.03	1.25	-	-	0.01	0.76
		Marine	0.01	0.03	-	0.42	-	-	0.00	1.39

Note. Sulfate & BB represents sulfate & biomass burning. VE represents vehicular emissions. ROC represents residual oil combustion. WI & IE represents waste incineration & industrial emissions. CC represents coal combustion. Absolute source concentrations are reported with two decimal places to accurately represent low concentration values and to avoid reporting 0.0 ng m^{-3} for non-zero concentrations. This provides a more precise dataset for reference. The main text adheres to the one-decimal-place convention for consistency in presentation.

References

Chang, Y., Huang, K., Xie, M., Deng, C., Zou, Z., Liu, S., and Zhang, Y.: First long-term and near real-time measurement of trace elements in China's urban atmosphere: Temporal variability, source apportionment and precipitation effect. Atmos. Chem. Phys., 18, 11793-11812. https://doi.org/10.5194/acp-18-11793-2018, 2018.

Chen, J., Tan, M., Li, Y., Zheng, J., Zhang, Y., Shan, Z., Zhang, G., and Li, Y.: Characteristics of trace elements and lead isotope ratios in PM2.5 from four sites in Shanghai, J. Hazard. Mater., 156, 36-43, https://doi.org/10.1016/j.jhazmat.2007.11.122, 2008.

Hsieh, C. -C., You, C. -F., & Ho, T. -Y.: The solubility and deposition flux of East Asian aerosol metals in the East China Sea: The effects of aeolian transport processes. Mar. Chem., 253, 104268. https://doi.org/10.1016/j.marchem.2023.104268, 2023.

Li, P., Li, Q., Shi, J., Gao, H., and Yao, X.: Concentration, solubility, and dry deposition flux of trace elements in fine and coarse particles in Qingdao during summer (in Chinese), Environ. Sci., 39, 3067-3074, https://doi.org/10.13227/j.hjkx.201712231, 2018.

Ming, L., Jin, L., Li, J., Fu, P., Yang, W., Liu, D., Zhang, G., Wang, Z., and Li, X.: PM2.5 in the Yangtze River Delta, China: Chemical compositions, seasonal variations, and regional pollution events. Environ. Pollut., 223, 200-212, https://doi.org/10.1016/j.envpol.2017.01.013, 2017.

Sun. H., Sun, J., Zhu, C., Yu, L., Lou, Y., Li, R., and Lin, Z.: Chemical characterizations and sources of PM2.5 over the offshore Eastern China sea: Water soluble ions, stable isotopic compositions, and metal elements. Atmos. Pollut. Res., 13, 101410, https://doi.org/10.1016/j.apr.2022.101410, 2022.

Taylor, S. R.: Trace element abundances and the chondritic earth model, Geochim. Cosmochim. Ac., 28, 1989-1998, https://doi.org/10.1016/0016-7037(64)90142-5, 1964.

Tian, H., Liu, K., Zhou, J., Lu, L., Hao, J., Qiu, P., Gao, J., Zhu, C., Wang, K., and Hua, S.: Atmospheric Emission Inventory of Hazardous Trace Elements from China's Coal-Fired Power Plants-Temporal Trends and Spatial Variation Characteristics, Environ. Sci. Technol., 48, 3575-3582, http://doi.org/10.1021/es404730j, 2014.

Wang, Y., Cheng, K., Tian, H.-Z., Yi, P., and Xue, Z.-G.: Emission Characteristics and Control Prospects of Primary PM2.5 from Fossil Fuel Power Plants in China, Aerosol Air Qual. Res., 16, 3290-3301, http://doi.org/10.4209/aaqr.2016.07.0324, 2016.

Wu, C., Huang, X. H. H., Ng, W., Griffith, S. M., and Yu, J. Z.: Inter-comparison of NIOSH and IMPROVE protocols for OC and EC determination: implications for inter-protocol data conversion, Atmos. Meas. Tech., 9, 4547-4560, https://doi.org/10.5194/amt-9-4547-2016, 2016.

Wu, S. P., Cai, M. J., Xu, C., Zhang, N., Zhou, J. B., Yan, J. P., Schwab, J. J., and Yuan, C. S.: Chemical nature of PM2.5 and PM10 in the coastal urban Xiamen, China: Insights into the impacts of shipping emissions and health risk, Atmos. Environ., 227, https://doi.org/10.1016/j.atmosenv.2020.117383, 2020.

Yang, F., Tan, J., Zhao, Q., Du, Z., He, K., Ma, Y., Duan, F., Chen, G., and Zhao, Q.: Characteristics of PM2.5 speciation in representative megacities and across China, Atmos. Chem. Phys., 11, 5207-5219, https://doi.org/10.5194/acp-11-5207-2011, 2011.

Yang, T., Chen, Y., Zhou, S., Li, H., Wang, F., and Zhu, Y.: Solubilities and deposition fluxes of atmospheric Fe and Cu over the Northwest Pacific and its marginal seas, Atmos. Environ., 239, 117763, https://doi.org/10.1016/j.atmosenv.2020.117763, 2020.

Yen, P. -H., Yuan, C. -S., Ceng, J. -H., Chiang, K. -C., Tseng, Y. -L., Soong, K. -Y., and Jeng, M. -S.: Inter-comparison of chemical fingerprint and source apportionment of marine fine particles at two islands through the west and east passages of the Taiwan Island. Sci. Total Environ., 851, 158313. http://dx.doi.org/10.1016/j.scitotenv.2022.158313, 2022.

Yen, P. -H., Yuan, C. -S., Wu, C. -H., Yeh, M. -J., Tseng, Y. -L., Soong, K. -Y.: Transport route-based cluster analysis of chemical fingerprints and source origins of marine fine particles (PM2.5) in South China Sea. Sci. Total Environ., 806, 150591. https://doi.org/10.1016/j.scitotenv.2021.150591, 2022.

Yuan, C. -S., Hung, C. -M., Hung, K. -N., Yang, Z. -M., Cheng, P. -H., and Soong, K. -Y.: Route-based chemical significance and source origin of marine PM2.5 at three remote islands in East Asia: Spatiotemporal variation and long-range transport. Atmos. Pollut. Res., 14, 101762. https://doi.org/10.1016/j.apr.2023.101762, 2023.

Zhang, H., Li, R., Dong, S., Wang, F., Zhu, Y., Meng, H., Huang, C., Ren, Y., Wang, X., Hu, X., Li, T., Peng, C., Zhang, G., Xue, L., Wang, X., and Tang, M.: Abundance and Fractional Solubility of Aerosol Iron During Winter at a Coastal City in Northern China: Similarities and Contrasts Between Fine and Coarse Particles, J. Geophys. Res.-Atmos., 127, https://doi.org/10.1029/2021JD036070, 2022.

Zhang, L., Gao, Y., Wu, S., Zhang, S., Smith, K. R., Yao, X., and Gao, H.: Global impact of atmospheric arsenic on health risk: 2005 to 2015, P. Natl. Acad. Sci. USA, 117, 13975-13982, https://doi.org/10.1073/pnas.2002580117, 2020.

Zhang, W., Peng, X., Bi, X., Cheng, Y., Liang, D., Wu, J., Tian, Y., Zhang, Y., and Feng, Y.: Source apportionment of PM2.5 using online and offline measurements of chemical components in Tianjin, China. Atmos. Environ., 244, 117942. https://doi.org/10.1016/j.atmosenv.2020.117942, 2021.

Zhao, R., Han, B., Lu, B., Zhang, N., Zhu, L., and Bai, Z.: Element composition and source apportionment of atmospheric aerosols over the China Sea. Atmos. Pollut. Res., 6, 191-201. http://doi.org/10.5094/APR.2015.023, 2015.

Zhu, Y., Li, W., Wang, Y., Zhang, J., Liu, L., Xu, L., Xu, J., Shi, J., Shao, L., Fu, P., Zhang, D., and Shi, Z.: Sources and processes of iron aerosols in a megacity in Eastern China, Atmos. Chem. Phys., 22, 2191-2202. https://doi.org/10.5194/acp-22-2191-2022, 2022.